J-PLUS: Two-dimensional analysis of the stellar population in NGC 5473 and NGC 5485

I. San Roman[1], P. Sánchez-Blázquez[2], A. J. Cenarro[1], L. A. Díaz-García[1], C. López-Sanjuan[1], J. Varela[1],
G. Vilella-Rojo[1], S. Akras[3], S. Bonoli[1], A. L. Chies Santos[4], P. Coelho[5], A. Cortesi[5], A. Ederoclite[1],
Y. Jiménez-Teja[3], R. Logroño-García[1], R. Lopes de Oliveira[6,3,7,8], J. P. Nogueira-Cavalcante[3], A. Orsi[1],
H. Vázquez Ramió[1], K. Viironen[1], D. Cristóbal-Hornillos[1], R. Dupke[3], A. Marín-Franch[1], C. Mendes de Oliveira[5],
M. Moles[1], and L. Sodré[5]

[1] Centro de Estudios de Física del Cosmos de Aragón (CEFCA), Unidad Asociada al CSIC, Plaza San Juan 1, 44001 Teruel, Spain
  e-mail: `isanroman@cefca.es`
[2] Departamento de Física Teórica, Universidad Autonoma de Madrid (UAM-CSIC), 28049 Cantoblanco, Madrid, Spain
[3] Observatório Nacional/MCTI, Rua Gal. José Cristino, 77, São Cristóvão, 20921-400 Rio de Janeiro, RJ, Brazil
[4] Departamento de Astronomia, Instituto de Física, Universidade Federal do Rio Grande do Sul (UFRGS), Porto Alegre, RS, Brazil
[5] Instituto de Astronomia, Geofísica e Ciências Atmosféricas (IAG), Universidade de São Paulo (USP), R. do Matão 1226,
  05508-090 São Paulo, Brazil
[6] Departamento de Física, Universidade Federal de Sergipe, Av. Marechal Rondon s/n, 49000-000 São Cristóvão, SE, Brazil
[7] X-ray Astrophysics Laboratory, NASA Goddard Space Flight Center, Greenbelt, MD 20771, USA
[8] Department of Physics, University of Maryland, Baltimore County, 1000 Hilltop Circle, Baltimore, MD 21250, USA

ABSTRACT

Context. The spatial variations of stellar population properties within a galaxy are intimately related to their formation process. Therefore, spatially resolved studies of galaxies are essential to uncover their formation and assembly. Although the arrival of integral field unit (IFU) surveys has brought a significant breakthrough in the field, recent techniques that combine photometric multifilter surveys with spectral fitting diagnostics have opened a new, relatively low-cost way to disentangle the stellar population of spatially resolved galaxies compared to IFU surveys.
Aims. The Javalambre Photometric Local Universe Survey (J-PLUS) is a dedicated multifilter designed to observed ~8500 deg^2 of the northern sky using 12 narrowband, intermediate-band, and broadband filters in the optical range. In this study, we test the potential of the multifilter observation carried out with J-PLUS to investigate the properties of spatially resolved nearby galaxies.
Methods. We present detailed 2D maps of stellar population properties, i.e., age, metallicity, extinction, and stellar mass surface density, for two early-type galaxies observed in the J-PLUS and CALIFA surveys. These galaxies are NGC 5473 and NGC 5485. Radial structures are also compared and luminosity- and mass-weighted profiles are derived. We use MUFFIT to process the J-PLUS photometric multifilter observations, and STARLIGHT and STECKMAP to analyze IFU CALIFA data.
Results. We demonstrate the scientific potential of J-PLUS/MUFFIT to explore the spatially resolved stellar populations of local galaxies. We find significant discrepancies between the results from the various analysis methods. While radial stellar population gradients obtained with J-PLUS/MUFFIT and the IFU technique CALIFA/STECKMAP are more in agreement, radial stellar population gradients largely differ when CALIFA/STARLIGHT methodology is used. A comparison of the absolute values reveals the existence of intrinsic systematic differences. Age and metallicity radial profiles derived from J-PLUS/MUFFIT are very similar when luminosity- or mass-weighted properties are used, suggesting that the contribution of a younger component is small and the star formation history of these early-type galaxies are well represented by mainly an old single stellar population component.
Conclusions. We present the potential of J-PLUS to explore the unresolved stellar populations of spatially extended local galaxies. A comparison between the three methodologies reveals some discrepancies suggesting that the specific characteristics of each method causes important differences. We conclude that the ages, metallicities, and extinction derived for individual galaxies not only depend on the chosen models but also depend on the method used. Future work is required to evaluate in detail the origin of these differences and to quantify the impact that different fitting routines have on the derived stellar population properties.

Key words. galaxies: evolution – galaxies: formation – galaxies: photometry – galaxies: elliptical and lenticular, cD –
galaxies: stellar content

1. Introduction

The study of the stellar content of galaxies is crucial to unveil their formation and assembly. In the last 15 years, the field has witnessed the outbreak of integral field spectroscopy (IFS) surveys (SAURON, de Zeeuw et al. 2002; VENGA, Blanc et al. 2010; PINGS, Rosales-Ortega et al. 2010; DiskMass, Bershady et al. 2010; ATLAS^{3D}, Cappellari et al. 2011; CALIFA, Sánchez et al.

2012). While large surveys of galaxies such as the Sloan Digital Sky Survey (SDSS; York et al. 2000), the Galaxy and Mass Assembly project (GAMA; Driver et al. 2011), or the 2dF Galaxy Redshift Survey (2dFGRS; Colless et al. 2001) obtain one spectrum per galaxy, IFS surveys spectrally map galaxies pixel by pixel. These IFS surveys allow detailed spatial analyses through multiple spectra of each galaxy by creating a 2D map of the object. While these surveys are very powerful, they are still

limited in the number of galaxies and redshift range; for example, CALIFA observes ~650 galaxies with redshifts limited to $z < 0.03$. Currently, a new generation of multiplexed IFS surveys, which can observe many galaxies simultaneously, has become a reality (SAMI, Croom et al. 2012; MaNGA, Bundy et al. 2015). Although this technique has allowed for a significant increase in the number of galaxies, there are still limitations in terms of the redshift range probed and the galactocentric distance analyzed (i.e., few effective radii, $R_{\rm eff}$). For example, MaNGA aims to obtain spatially resolved spectroscopy of 10 000 galaxies but it will be limited to resolve galaxies spatially out to $R = 1.5\,R_{\rm eff}$ (with a subsample reaching $R = 2.5\,R_{\rm eff}$) and with a median redshift of $z \sim 0.03$ (Bundy et al. 2015). Redshifts are limited to $z < 0.095$ in the SAMI survey and the data typically reach $1.7\,R_{\rm eff}$ ($2\,R_{\rm eff}$ for 40% of the sample).

Recent hydrodynamical simulations have found that the information content of the accretion history is retained in the stellar population profiles only at very large radii ($R > 2R_{\rm eff}$) from the galactic center (Cook et al. 2016). The limitations of current IFU surveys at these low signal-to-noise (S/N) regimes suggest that deep photometric studies in galactic stellar halos are essential to unveil the formation and assembly of local galaxies.

On the other hand, the number of alternative techniques such as multifilter surveys is significantly increasing (e.g., COMBO-17, Wolf et al. 2003; ALHAMBRA, Moles et al. 2008; PAU, Castander et al. 2012; SHARDS, Pérez-González et al. 2013: J-PAS, Benitez et al. 2014; J-PLUS, Cenarro et al. 2019, hereafter Paper I). These photometric surveys aim at a diversity of scientific goals but with a common characteristic: a well-sampled spectral energy distribution (SED) of galaxies using broadband, intermediate-band, or narrowband filters in the optical range. Halfway between classical photometry and standard spectroscopy, these retrieved SEDs are effectively spectra with a low-spectral resolution depending on the filter system (e.g., $R \sim 20$ for ALHAMBRA; $R \sim 50$ for J-PAS). Although multifilter observing techniques suffer from a lack of high spectral resolution, these techniques have multiple advantages over standard spectroscopy as follows: 1) IFU-like character, allowing a pixel-by-pixel investigation of extended galaxies; 2) a uniform and nonbiased spatial sampling that allows environmental studies; 3) larger galaxy samples than multiobject spectroscopic surveys; 4) no sample selection criteria other than the photometric depth in the detection band; and 5) analysis of lower brightness surface areas than in spectroscopy, allowing the studies of the outermost regions of the galaxies and of galaxies at higher redshifts. That is, multifilter surveys are generally deeper than traditional spectroscopic studies since direct imaging is more efficient than spectroscopy. These surveys also allow studies of very nearby galaxies ($z < 0.01$) that are too spatially extended to be suitable for the small field of view of current IFU surveys. In this context multifilter surveys open a way to improve our knowledge of galaxy formation and evolution that complements standard multiobject spectroscopic surveys.

San Roman et al. (2018) developed a novel technique to analyze unresolved stellar populations of spatially resolved galaxies based on photometric multifilter surveys. In that work, we applied the technique to a sample of 29 massive ($M_\star > 10^{10.5}\,M_\odot$) early-type galaxies at $z < 0.3$ from the ALHAMBRA survey (Moles et al. 2008) to derive stellar population and extinction gradients out to 2–$3.5\,R_{\rm eff}$. We found, on average, flat luminosity-weighted age gradients ($\nabla\log\,{\rm Age}_{\rm L} = 0.02 \pm 0.06\,{\rm dex}/R_{\rm eff}$) and negative luminosity-weighted gradients in metallicity ($\nabla{\rm [Fe/H]}_{\rm L} = -0.09 \pm 0.06\,{\rm dex}/R_{\rm eff}$).

Although these results are in agreement with previous long-slit analyses (e.g., Mehlert et al. 2003; Sánchez-Blázquez et al.

2006, 2007; Reda et al. 2007; Spolaor et al. 2010) and also with the most recent IFU studies (e.g., Rawle et al. 2008, 2010; Kuntschner et al. 2010; Wilkinson et al. 2015; Goddard et al. 2017), they are discrepant when compared with some recent results. Most studies in the literature have found either flat or slightly positive age gradients in early-type galaxies, however recent IFU works present disparate results (see Table 3 in San Roman et al. 2018, for a comprehensive review). In particular, the results of González Delgado et al. (2015) found, using a sample of 41 early-type galaxies from the CALIFA survey, very negative inner ($<R_{\rm eff}$) luminosity-weighted age gradients ($\sim$–0.25 dex/$R_{\rm eff}$) that become flatter ($\sim$–0.05 dex/$R_{\rm eff}$) at larger galactocentric distances (up to $2\,R_{\rm eff}$). Most recently, Boardman et al. (2017) observed 12 H I-detected early-type galaxies and found median age gradients of -0.047 dex/dex (in log-space), reaching approximately 3 half-light radii. Studies based on IFU MaNGA reveal contradictory results; while Goddard et al. (2017) found a flat age gradient inside $R < R_{\rm eff}$, Zheng et al. (2017) found a slightly negative gradient (-0.05 ± 0.01 dex/$R_{\rm eff}$). Both MaNGA studies analyzed similar galaxy samples but used different spectral fitting techniques and stellar population models. To shed light into this problem, in this paper we propose the analysis of common objects observed with the photometric multifilter J-PLUS and IFU CALIFA but analyzed with different techniques.

The Javalambre Photometric Local Universe Survey (J-PLUS, Paper I) is a photometric multi-filter survey defined to observe $\sim$8500 deg^2 of the northern sky. A combination of J-PLUS observations with spectral fitting diagnostics will disentangle the stellar population of spatially extended galaxies. In contrast, the Calar Alto Legacy Integral Field Area (CALIFA) survey is a pioneer in the integral field spectroscopy legacy projects. Recent studies using data from CALIFA provided the most comprehensive results so far regarding the radial variations of the stellar population parameters and star formation histories of nearby galaxies (e.g., Pérez et al. 2013; Sánchez et al. 2014; Sánchez-Blázquez et al. 2014).

The specific goals of this paper are to illustrate the potential of J-PLUS to analyze unresolved stellar populations of spatially extended local galaxies and to compare our method (MUFFIT, Díaz-García et al. 2015) applied to J-PLUS data with two different methods applied to CALIFA data: i.e., STARLIGHT (Cid Fernandes et al. 2013) and STECKMAP (Ocvirk et al. 2006a,b).

This paper is organized as follows. Section 2 provides a brief overview of the J-PLUS Science Verification Data (SVD) and the CALIFA survey as well as the photometric properties of our sample. In Sect. 3, we describe the technical aspects of the methods used to analyze the different data sets. Section 4 presents the J-PLUS and CALIFA 2D maps of age, [Fe/H], $A_{\rm v}$, and stellar mass density and Sect. 5 presents the radial profiles and gradients. The stellar mass-to-light ratio analysis and the integrated properties of the sample are presented in Sects. 6 and 7, respectively. We discuss the results in Sect. 8. Throughout this paper we assume a ΛCDM cosmology with $H_0 = 70\,{\rm km\,s^{-1}}$, $\Omega_{\rm M} = 0.30$, and $\Omega_\Lambda = 0.70$.

2. Observations and data reduction

2.1. J-PLUS SVD

The J-PLUS is a multifilter survey carried out with the Javalambre Auxiliary Survey Telescope (JAST/T80), a 0.83 m telescope installed at the Observatorio Astrofísico de Javalambre (OAJ) in Teruel, Spain. The survey uses the panoramic camera T80Cam

that provides a large field of view of $2\,\text{deg}^2$ with a pixel scale of $0.55''\,\text{pixel}^{-1}$. Primarily, J-PLUS was conceived to perform the calibration tasks for the main J-PAS[1] survey that will observe a contiguous area of $8500\,\text{deg}^2$. The specially designed filter system covers the optical range with 12 broadband, intermediate-band, and narrowband filters. The photometric filter set is composed of 4 broadband (g, r, i, and z), 2 intermediate-band (u and $J0861$), and 6 narrowband ($J0378$, $J0395$, $J0410$, $J0430$, $J0515$, and $J0660$) filters optimized to provide an adequate sampling of the SED. Figure 3 in Paper I shows the transmission curves of the complete set of filters. The final survey parameters and scientific goals, as well as the technical requirements of the filter set, are described in Paper I. In this paper, we make use of observations collected during the science verification phase of J-PLUS (1500041, P.I.: G. Vilella). These observations are available through the J-PLUS web page[2] and are part of J-PLUS early data release (EDR). In addition to the present paper, the J-PLUS EDR and SVD have so far been used to refine the membership in nearby galaxy clusters (Molino et al. 2019), analyze the globular cluster M15 (Bonatto et al. 2019), study the Hα emission of several local galaxies (Logroño-García et al. 2019), and compute the stellar and galaxy number counts up to $r = 21$ (López-Sanjuan et al. 2019).

The data processing and calibration is carried out using an automated pipeline developed and implemented at the Centro de Estudios del Cosmos de Aragón (CEFCA)[3]. The data processing includes standard steps such as overscan subtraction, flat-field correction, and rejections of bad pixels and cosmic rays. If needed, fringe corrections are applied to the images. The pipeline makes use of the packages `Scamp` (Bertin 2006) and `Swarp` (Bertin et al. 2002) to perform the astrometric calibration and image coadding. The photometric calibration is performed through a series of calibration procedures (e.g., based on SDSS observations and spectrophotometric standard stars) rather than relying on a single calibration technique. More technical details involved in the data processing and calibration procedure can be found in Paper I. Table 1 summarizes the journal of observations and provides basic information on the filters used. We note that because of the science verification nature of the observations, the exposure times are different from the general observation conditions of J-PLUS. In spite of these peculiarities, SVD is representative of the whole J-PLUS survey and analyses presented in this paper are directly applicable to future 2D J-PLUS studies (see details in Paper I).

The target sample of this paper was selected exclusively to study common objects observed with both J-PLUS and CALIFA surveys. For the purposes of this early paper, we focus on the analysis of spheroidal, large, and bright galaxies. This selection criteria restrict this work to the study of the only two early-type galaxies, NGC 5473 and NGC 5485. We note that there are no objects in common between J-PLUS and any other IFU survey at the moment (e.g., MaNGA DR14, SAMI DR1, Sauron) except for CALIFA and ATLAS[3D]. The ATLAS[3D] survey also presents IFU data for the two objects analyzed in this paper. Although no direct

Table 1. J-PLUS SVD observation summary.

Filter	λ_{eff} (nm)	$\Delta\lambda_{\text{eff}}$ (nm)	Exp. time (s)	$FWHM_{\text{mean}}$ (arcsec)
u	348.5	50.8	3×207	1.49
$J0378$	378.5	16.8	3×200	1.28
$J0395$	395.0	10.0	3×98	1.23
$J0410$	410.0	20.0	3×39	1.25
$J0430$	430.0	20.0	3×37	1.69
g	480.3	140.9	3×52	1.15
$J0515$	515.0	20.0	3×41	1.13
r	625.4	138.8	3×80	1.16
$J0660$	660.0	13.8	3×270	1.15
i	766.8	153.5	3×26	1.23
$J0861$	861.0	40.0	3×270	1.13
z	911.4	140.9	3×36	1.05

Notes. Column 1: filter name; Col. 2: central wavelength; Col. 3: effective pass band; Col. 4: exposure time; Col. 5: mean full width at half maximum.

comparison is made with these observations owing to the limited area covered ($<1\,R_{\text{eff}}$) and small wavelength range (480–538 nm) of ATLAS[3D], a qualitative comparison is made in Sect. 5. Table 2 summarizes the basic properties of the two objects analyzed in this study. Figure 1 shows the J-PLUS color images of these objects. Visual inspection of Fig. 1 shows that while NGC 5473 looks like a classical early-type galaxy, NGC 5485 is a more complex galaxy with a prominent minor-axis dust lane.

2.2. CALIFA

CALIFA (Sánchez et al. 2012) is a pioneer wide-field IFS survey of 667 galaxies in the local universe. The observations were carried out with the Potsdam Multi-Aperture Spectrometer (PMAS; Roth et al. 2005) in the PPaK mode (Verheijen et al. 2004) at the 3.5 m telescope of Calar Alto observatory. PPaK contains 382 fibers of $2.7''$ diameter each and a $74'' \times 64''$ field of view. Three different spectral setups are available: i) a low-resolution V500 setup covering the wavelength range 3745–7500 Å with a spectral resolution of 6.0 Å (FWHM); ii) a medium-resolution V1200 setup covering the wavelength range 3650–4840 Å with a spectral resolution of 2.3 Å (FWHM); and iii) the combination of the cubes from both, i) and ii), setups (called COMBO) with a spectral resolution of 6.0 Å and a wavelength range between 3700–7500 Å. The target sample has been selected from the photometric catalog of SDSS (York et al. 2000) as a sample limited in the apparent isophotal diameter, $45'' < \text{iso}A_r < 80''$, to fill the field of view of PPaK and cover the redshift range $0.005 < z < 0.03$. We refer to Sánchez et al. (2012, 2016) for details on the observational strategy and data processing. The COMBO data cubes of the two objects analyzed in this paper are available through the CALIFA website[4] and belong to the CALIFA DR3.

3. Method

Three different methods are used throughout this work: one single method to process the photometric multifilter observations (J-PLUS/MUFFIT), and two different techniques to analyze IFU CALIFA data (CALIFA/STARLIGHT and CALIFA/STECKMAP).

---

[1] The Javalambre Physics of the Accelerating Universe Astrophysical Survey (J-PAS) is a very wide-field cosmological survey to be conducted from the OAJ with the 2.5 m Javalambre Survey Telescope, JST/T250, and the panoramic camera JPCam ($4.7\,\text{deg}^2$ field of view). It will cover $8500\,\text{deg}^2$ with an unprecedented filter set of 54 contiguous, narrowband optical filters (145 Å width each, placed ~100 Å apart) plus 2 broadband filters at the blue and red sides of the optical range, and 3 SDSS-like filters.

[2] http://j-plus.es/datareleases

[3] http://www.cefca.es/

[4] http://califa.caha.es/
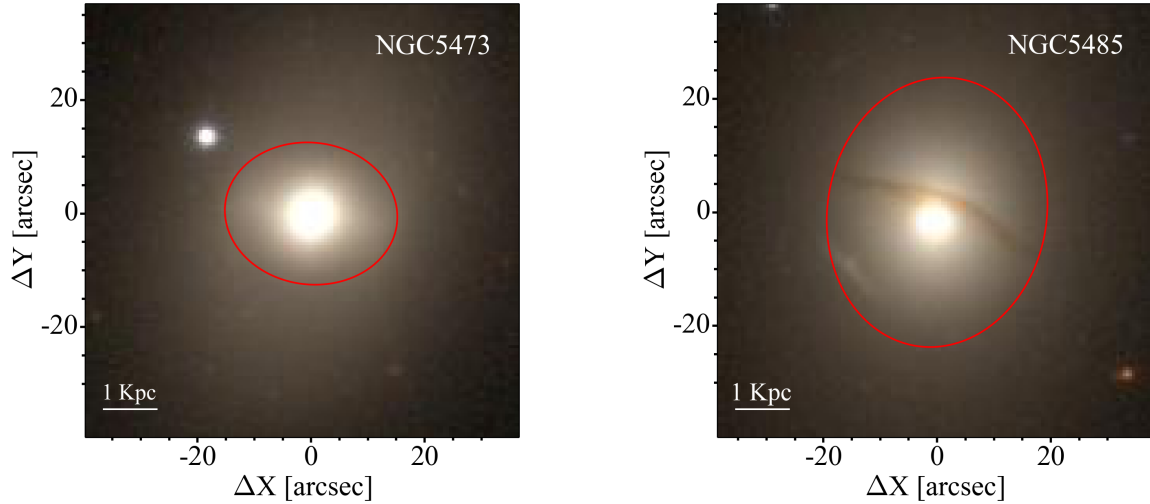
Fig. 1. J-PLUS colored composite images of the objects analyzed in this paper. The red solid line in each panel delimits a ellipse with the semimajor axis $R = 3\,R_{\mathrm{eff}}$.

Table 2. Objects general properties.

Object	CALIFA ID	RA (J2000.0)	Dec (J2000.0)	Hubble type	Environment	$M_B{}^a$	Redshift[b]	$\log M_{\mathrm{JAM}}{}^c$ ($M_\odot$)
NGC 5473	703	14:04:43.22	+54:53:33	E-S0	Isolated	−20.21	0.006	11.09
NGC 5485	708	14:07:11.37	+55:00:06	S0	Isolated	−19.89	0.006	11.05

Notes. Basic parameters from HyperLeda. [a]B-band absolute magnitude. [b]Spectroscopic redshift from SDSS. [c]Dynamical mass inferred from ATLAS[3D] survey (Cappellari et al. 2013).

Single stellar population (SSP) models are critical to disentangle physical properties of galaxies stellar populations. They are the basis on which to transform observed quantities into physical properties and involve choices among different initial mass functions, stellar libraries, and isochrones. Although several studies show a general good agreement when using different model sets, some evidence indicates systematic differences associated with the different SSP models used (e.g., Coelho et al. 2009; Dias et al. 2010; Cid Fernandes et al. 2014; Díaz-García et al. 2015; San Roman et al. 2018). To minimize the differences between the methods, we performed the comparison between the three methods described above using the same stellar population models (Bruzual & Charlot 2003, BC03 hereafter) except for CALIFA/STARLIGHT, which uses BC03 updated version Bruzual (2007, priv. commun.)[5]. These SSPs are an update of BC03 models, where STELIB (Le Borgne et al. 2003) is replaced by the MILES (Sánchez-Blázquez et al. 2006) and GRANADA (Martins et al. 2005; González Delgado et al. 2005) stellar libraries. In addition, the updated version incorporates an improved TP-AGB treatment (Marigo & Girardi 2007). Maraston et al. (2006) have shown that the treatment of the TP-AGB phase of stellar evolution is a source of discrepancy in the determination of the spectroscopic age and mass of high-z ($1.4 < z < 2.7$) galaxies. Although the results inferred using different prescriptions show significant differences in the infrared, major discrepancies are not expected in the optical regime (e.g., Bruzual 2007; Röck et al. 2016). We selected the Padova 1994 tracks (Bressan et al. 1993; Fagotto et al. 1994a,b; Girardi et al. 1996), which cover a range of ages from 0.001 to 14 Gyr and metallicities [Fe/H] = −2.3, −1.7, −0.7, −0.4, 0.0,

+0.4. A Chabrier (2003) initial mass function has been used in all the cases.

3.1. J-PLUS/MUFFIT

The method used in this analysis has been extensively described and tested in San Roman et al. (2018). It can be summarized in three main steps: the homogenization of the point-spread functions (PSF), the spatial binning of the images through a centroidal Voronoi tessellation (CVT; Cappellari & Copin 2003), and the SED fitting of each bin. For the SED fitting, we used the code MUFFIT (MUlti-Filter FITting for stellar population diagnostics; Díaz-García et al. 2015). A generic code, MUFFIT is optimized to retrieve the main stellar population parameters of galaxies in photometric multifilter surveys.

To perform good-quality multicolor photometry of such wide field of view, PSF homogenization processes are required. The PSF variations cause the light inside a given aperture to be redistributed differently across the field of view and from filter to filter. These effects may produce artificial structures that could bias our results (Bertin 2011). To avoid this problem, we performed a PSF homogenization in the 12 bands. We used `SExtractor` (Bertin & Arnouts 1996) and `PSFEx` (Bertin 2013) in every image to generate a homogenization kernel, where the worst (widest) PSF value of the image set was chosen as a target PSF. A 2D Moffat model is used as a homogenization kernel. The images were convolved with their corresponding kernels using a fast Fourier transform, bringing the images of all the bands to the same circular PSF. Finally, we took into account that the homogenization process affects the image noise, producing pixel-by-pixel correlations. To correct for this, we recalculated the noise model of the images using the procedure described in

---

[5] The Bruzual (2007) models are available at `http://www.bruzual.org/~gbruzual/cb07`

Labbé et al. (2003) and Molino et al. (2014). We then used this recalculated noise model to compute the photometric errors.

To ensure a reliable determination of the stellar population parameters we performed a CVT imposing a minimum S/N of 10 in the $J0378$ filter. We chose this filter because, for the selected targets, it is the one with the lowest S/N. We note that this choice is a conservative limit and that slightly lower S/N could extended the analysis to larger galactocentric radii (e.g., sacrificing the S/N of 1 out of 12 filters). As mentioned in the introduction, multifilter techniques allow the analysis of galaxy profiles at larger galacto-centric radii and at higher redshift than spectroscopic surveys.

Although overall this idea is true and IFU-like photometric techniques can map fainter surface brightness levels, for this specific study we have been conservative and only the pixels inside the Kron radius of the blue filter J0378, R_{Kron}, were included in the analysis. The value R_{Kron} is defined by SExtractor as a flexible elliptical aperture that confines most of the flux from an object and has been empirically tested to enclose >90% of the object light.

A comprehensive study of MUFFIT performance on J-PLUS and the dependency with the S/N of each filter is out of the scope of this paper and will be presented in a future work. The tessellation was then applied to the images in all the filters, and finally, the photometry of every region in all the filters was determined. For details about the tessellation method see San Roman et al. (2018). J-PLUS images are already background subtracted. This subtraction is done globally over the entire image. To assure a good background subtraction, we further performed a local sky subtraction considering an area of 100×100 pixels ($55'' \times 55''$) around each target galaxy.

After performing the CVT and the photometry of every region in every filter is determined, we ran MUFFIT to obtain 2D maps of different stellar population properties. The code compares the multifilter fluxes of galaxies with the synthetic photometry of mixtures of two SSPs for a range of redshifts and extinctions through an error-weighted χ^2 approach. Several studies have shown that the mixture of two SSPs is a suitable and reliable approach to describe the stellar populations of early-type galaxies (Rogers et al. 2010; Ferreras & Silk 2000; Kaviraj et al. 2007; Lonoce et al. 2014). More recently, López-Corredoira et al. (2017) fit a set of 20 red galaxies with models of a single-burst SSP, a combination of two SSPs, and an extended star formation history. They concluded that exponentially decaying extended star formation models (τ-models) slightly improve the fits (they have lower average reduced χ^2) with respect to single-burst models, but they are considerably worse than the two SSPs based fits ($\chi^2 > 20\%$ larger). They conclude that the models with two SSPs represent better red galaxies. Based on these studies, we consider that a 2-SSP model fitting approach is the best method for our specific work.

Throughout this work the Fitzpatrick reddening law has been used (Fitzpatrick 1999) with extinctions values A_V in the range of 0–3.1. This extinction law is suitable for dereddening any photospectroscopic data, such as J-PLUS (further details in Fitzpatrick 1999). To minimize the number of free fitting parameters we provide MUFFIT with a fixed redshift value. We used the spectroscopic redshifts determined by SDSS (Table 2). We note that in the future J-PLUS will provide accurate photo-redshift values for local galaxies (see details in Paper I).

3.2. CALIFA/STARLIGHT

The first method used to extract stellar population information from the CALIFA data cubes is based on a full spectral synthesis approach via the STARLIGHT code (Cid Fernandes et al. 2005). Previous to the spectral fitting, all spaxels containing light from spurious sources (e.g., foreground stars and background galaxies) are masked. The spaxels with $S/N < 3$ are also masked. The cubes are then segmented into Voronoi zones using the routine described in Cappellari & Copin (2003). The target S/N is set to 20, which leaves most of the spaxels inside one half-light radius unbinned.

The STARLIGHT code fits an observed spectrum in terms of a model built by a linear combination of SSPs from a base spanning different ages and metallicities. Dust effects are modeled as a foreground screen with a Cardelli et al. (1989) reddening law with $R_v = 3.1$. The spectral fits were performed in the rest-frame 3700–6850 Å interval where the main optical emission lines were masked ([OII], Hγ, Hβ, [OIII], HeI, [OI], Hα, [NII], [SII]). Because of its interstellar absorption component, the NaI doublet was also masked. A more detailed explanation about CALIFA/STARLIGHT process can be found in Cid Fernandes et al. (2013, 2014). The spectra were then processed through PYCASSO[6] (the Python CALIFA Starlight Synthesis Organizer; de Amorim et al. 2017) producing the results discussed in the next sections.

The star formation histories are derived with two different stellar population model: the Granada (Martins et al. 2005; González Delgado et al. 2005) and the Bruzual (2007, priv. comm.). We chose to compare the results with the latter as these models are very similar to those used in J-PLUS/MUFFIT and CALIFA/STECKMAP.

3.3. CALIFA/STECKMAP

The second method used to extract stellar population information from the CALIFA data cubes is based on a spectral feature synthesis approach using STECKMAP code (STEllar Content and Kinematics via Maximum A Posteriori likelihood; Ocvirk et al. 2006a,b). Previous to the spectral fitting, preprocessing steps include spatial masking of foreground/background sources, very low S/N spaxels, and bad pixels. Although CALIFA/STECKMAP spatially bins the data cubes using also the CVT routine describe in Cappellari & Copin (2003), the minimum S/N required is more restrictive (40 per Å at 5800 Å) than for the CALIFA/STARLIGHT method. This conservative restriction produces a different Voronoi segmentation than that used in CALIFA/STARLIGHT but ensures a reliable determination of the stellar population properties. The STECKMAP code is run on the emission lines cleaned spectra, where the emission line cleaning has been performed with the code GANDALF (Sarzi et al. 2006).

A Bayesian method, STECKMAP simultaneously recovers the kinematic and stellar population properties via a maximum a posteriori algorithm. The STECKMAP code projects the observed spectrum onto a temporal sequence of models of SSPs to determine the linear combination that better fits the observed spectrum. The stellar content of the object is indicated by the weights of the various components of this linear combination, thus the method does not assume the shape of the star formation history. The STECKMAP method uses a penalized χ^2 that imposes high penalization values for solutions with strong oscillations (i.e., a rapid variation of the metallicity with age or a noisy broadening function) and small penalization values for smoothly varying solutions. This initial condition avoids extreme oscillating solutions that are not robust and most likely

---

[6] `www.pycasso.iaa.es`

unphysical. We note that this method does not use the continuum in the derivation of the stellar population parameters. The model is multiplied by a smooth nonparametric transmission curve. This curve extends uniformly along the wavelength range. By using this curve to remove the continuum, no extinction correction needs to be applied as dust extinction does not change the equivalent width of the absorption lines. Therefore, an extinction law is not assumed. This technique avoids spurious results due to possible flux calibration errors or extinction. For details about the analysis method see Sánchez-Blázquez et al. (2011, 2014), while the performance of STECKMAP is described in Ocvirk et al. (2006a,b). The typical STECKMAP outputs give the proportion of stars at each age that are contributing to the observed flux and to the stellar mass and evolution of the metallicity with time.

4. Two-dimensional maps

As explained in the previous section, J-PLUS/MUFFIT and CALIFA/STARLIGHT provide luminosity- and mass-weighted log Age, [Fe/H], and A_v maps while we can obtain luminosity- and mass-weighted log Age and [Fe/H] maps from the CALIFA/STECKMAP outputs. Mass-weighted properties are more representative of the whole evolutionary history of the galaxy since they give insight into its mass assembly history. On the other hand, luminosity-weighted properties are better constrained and more sensitive to the fingerprints of the most recent periods of star formation in the galaxy. Throughout this study, we analyze both mass- and luminosity-weighted properties. We present the mass-weighted properties maps in this section. For completeness, Appendix A includes the luminosity-weighted maps.

4.1. Age, [Fe/H], A_v, and stellar mass surface density

Figures 2 and 3 show the 2D maps of the stellar populations for NGC 5473 and NGC 5485 derived with various methods. We shifted the maps to center the galaxies and facilitate the comparison. The center of each galaxy (white crosses in each 2D map) was derived using the IRAF task ELLIPSE to fit elliptical isophotes to the stellar mass surface density maps. We fitted the isophotes between 0.1 arcsec and the largest measurable semimajor axis. We determined the overall center position as the average of ELLIPSE output between 0.5 and 1.5 arcsec along the semimajor axis where the measurements are more reliable.

We anticipated that the J-PLUS/MUFFIT maps would expand to larger galactocentric radii (i.e., analysis of fainter surface brightness levels) but we restricted the analysis to the inner part of the galaxies owing to the scientific verification nature of this paper. For this specific study we were conservative: 1) only the pixels inside the Kron radius of the blue filter J0378 were included in the analysis, 2) a minimum S/N of 10 was imposed, and 3) all 12 filters were required. A comprehensive study of MUFFIT performance on J-PLUS and the dependency with the S/N of each filter is out of the scope of this paper and will be presented in a future work.

Figure 2 shows some differences between the values derived by each method. In the J-PLUS/MUFFIT maps NGC 5473 shows a smooth behavior in log Age_M, $[Fe/H]_M$, and A_v suggesting flat age and metallicity gradients. These results are in agreement with the relatively flat age and metallicity maps derived by CALIFA/STECKMAP. In contrast, CALIFA/STARLIGHT map suggests a mild negative age gradient. In addition, the upper

part of the galaxy seems to be more metal-rich than the lower part in the CALIFA/STARLIGHT metallicity map. Significant differences in the extinction parameter, A_v, are found between J-PLUS/MUFFIT and CALIFA/STARLIGHT. While J-PLUS/MUFFIT obtained a significant dust component, smoothly distributed within the galaxy, the CALIFA/STARLIGHT analysis found $A_v = 0$ across the whole galaxy except in the central region. We note that the older and metal-rich area (ΔX, $\Delta Y = -20''$, $15''$) visible in the CALIFA/STECKMAP corresponds to a background galaxy not masked during the preprocessing steps.

NGC 5485 (Fig. 3) also presents a relative smooth log Age_M and $[Fe/H]_M$ maps in J-PLUS/MUFFIT, but a higher extinction area ($A_v \sim 1.2$) at $-10'' \leq \Delta X \leq 10''$ and $0'' \leq \Delta Y \leq 10''$ is present in the A_v map. This high extinction could be associated with the prominent minor-axis dust lane visible in the colored images (Fig. 1). We note that the [Fe/H] map shows a slightly more metal-rich population in that specific area that could be produce by a potential metallicity-extinction degeneracy. The CALIFA/STARLIGHT analysis is also able to detect the prominent dust lane, although A_v values are significantly lower than the values obtained by J-PLUS/MUFFIT. The CALIFA/STECKMAP analysis shows smooth log Age_M, and $[Fe/H]_M$ maps, although this method obtains an older population. The log Age_M map determined by CALIFA/STARLIGHT exhibits an older component in the center of the galaxy not present in J-PLUS/MUFFIT or CALIFA/STECKMAP maps. This old component seems to have the same position, size, and orientation as the dust line crossing the galaxy. We checked that the general results do not significantly vary for luminosity-weighted parameters (see the luminosity-weighted maps in Appendix A). In a recent study, Martín-Navarro et al. (2018) have presented a spatially resolved stellar population analysis of a sample of 45 elliptical galaxies using the CALIFA survey. They have measured the stellar population properties (age, metallicity, and [Mg/Fe]) via a standard line-strength analysis of the indices $H\beta_o$, Fe4383, Fe5015, Fe5270, and Mgb (Worthey et al. 1994; Burstein et al. 1984). Overall, they have found flat age gradients and negative metallicity gradients. We note that their galaxy sample includes NGC 5485. Visual inspection of the NGC 5485 age map does not show any evidence for the old stellar component present in the CALIFA/STARLIGHT map.

A major concern regarding the A_v maps is the significant difference in dust extinction derived from the J-PLUS/MUFFIT and CALIFA/STARLIGHT analyses. Although several studies have supported our finding that the retrieved extinctions with MUFFIT are very robust (e.g., Díaz-García et al. 2015; San Roman et al. 2018) and that high values of $A_v \sim 0.8$ are not unusual in dusty early-type galaxies (Goddard et al. 2017; Wilkinson et al. 2015), this dust extinction difference need to be explored; see Sect. 4.2 for further discussion.

Although some degeneracies are unavoidable, analysis of their extension and the potential effects from these degeneracies are crucial in order to avoid any misinterpretation. To address the degeneracy problem, we used the stellar population values recovered by MUFFIT during the Monte Carlo approach for both objects in every bin of the tessellation. This approach assumes an independent Gaussian distribution in each filter, centered on the band flux or magnitude, and has a standard deviation equal to its photometric error. Figure 4 presents the 2D confidence intervals. The ellipses are obtained from the covariance matrix of each distribution following the method used in Díaz-García et al. (2015). A value of the ellipticity close
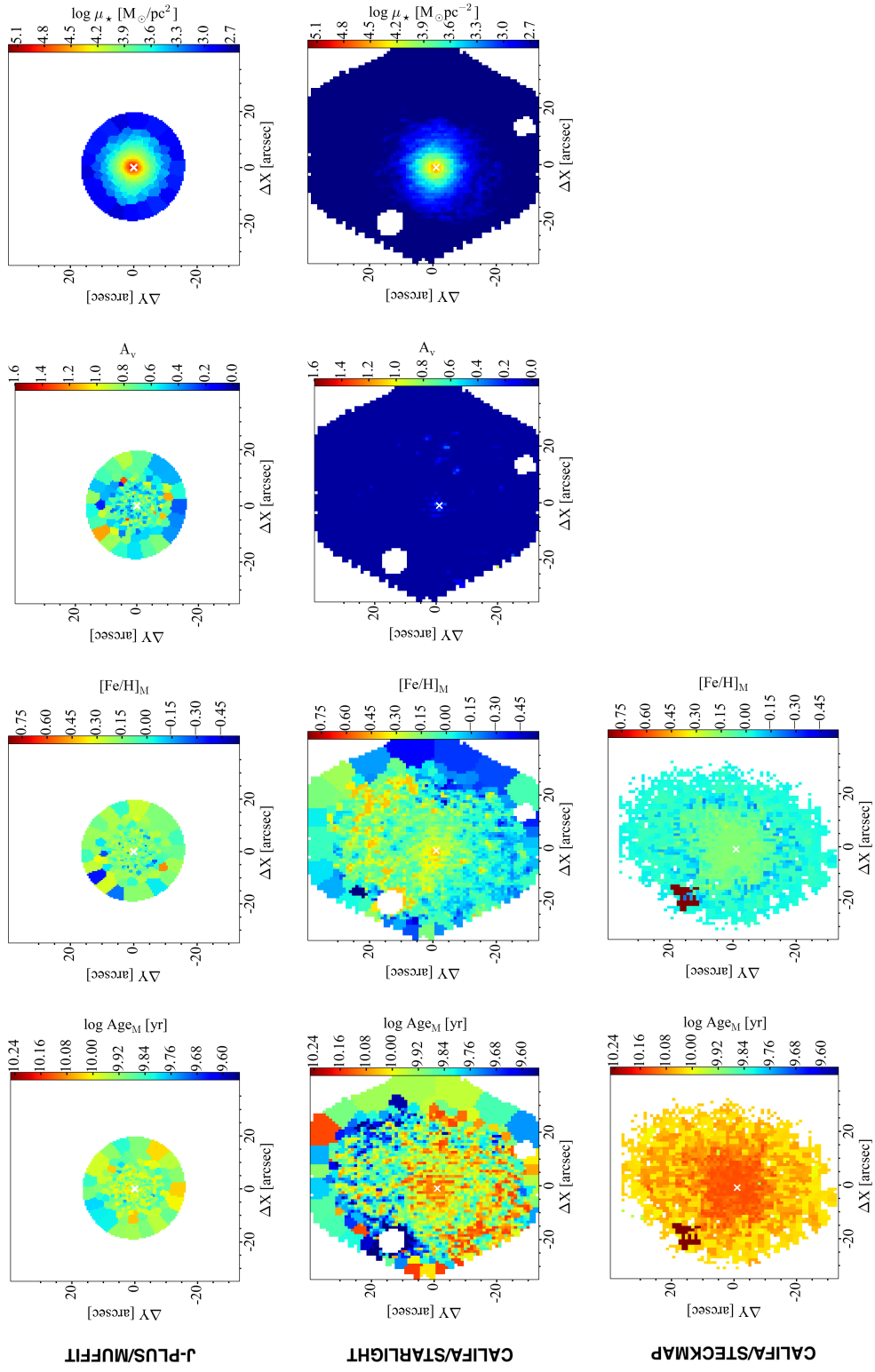
**Fig. 2.** Mass-weighted stellar population properties maps for NGC 5473 determined by J-PLUS/MUFFIT (*first row*), CALIFA/STARLIGHT (*second row*), and CALIFA/STECKMAP (*third row*). Each column corresponds to 2D maps for age (log Age), metallicity ([Fe/H]), extinction parameter (A_v), and stellar mass surface density (log $\mu_\star$). The color range is the same for the different methods. The center of the galaxy is indicated with a white cross in each panel.
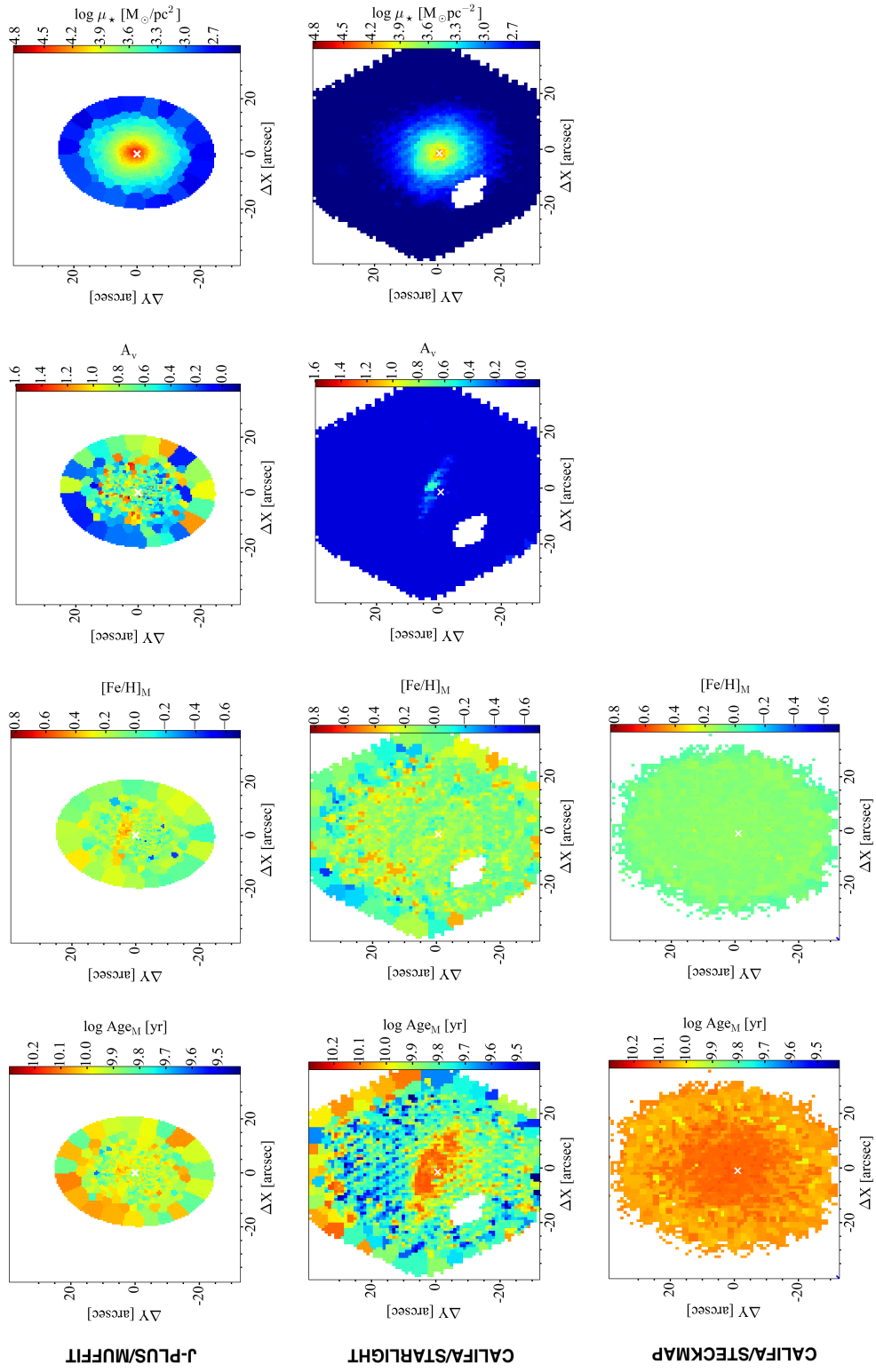
Fig. 3. Same as in Fig. 2, but for NGC 5485.
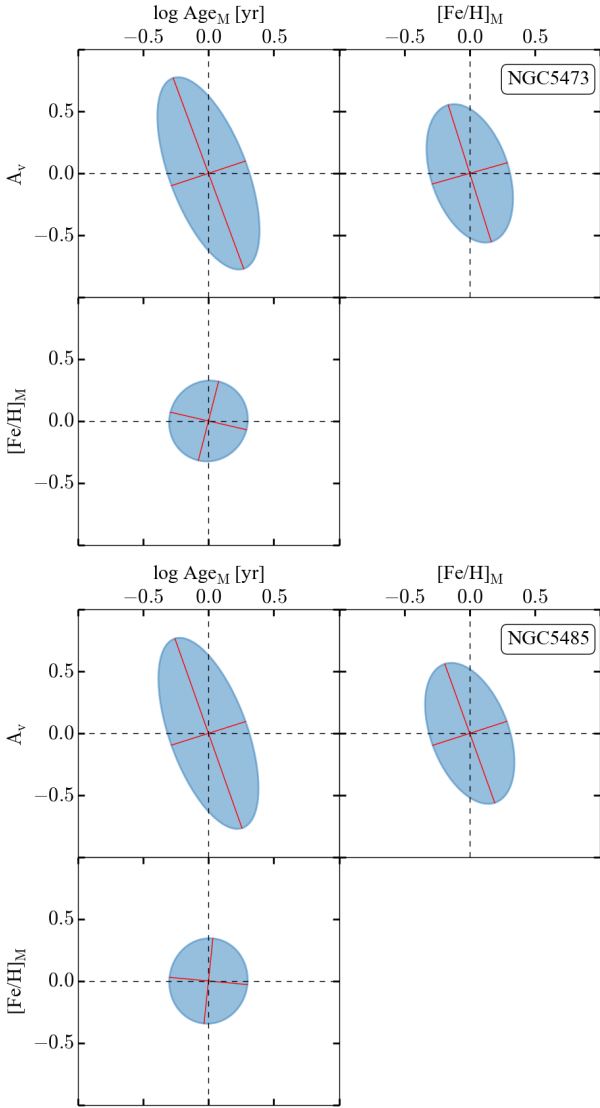
Fig. 4. Covariance error ellipses of the stellar population parameters for NGC 5473 (*top panel*) and NGC 5485 (*bottom panel*) using J-PLUS/MUFFIT.

to zero implies no degeneracy between the two parameters. Furthermore, when the position angle lies on any of the two axes (position angle multiple of $\pi/2$), the two parameters are not correlated and no degeneracy is found. Figure 4 shows no age-metallicity degeneracy but presents a degeneracy between A_v and the other two parameters. This means that a stellar population reddened by extinction can mimic a metal-rich or an old population. The J-PLUS/MUFFIT approach provides typical uncertainties of $\Delta \log \mathrm{Age}_M = 0.18$ dex, $\Delta [\mathrm{Fe/H}]_M = 0.3$ dex, and $\Delta A_v = 0.5$ for our specific target galaxies. These parameter errors are determined as the best solution space based on the Monte Carlo method. A comprehensive discussion about the intrinsic uncertainties and degeneracies of MUFFIT using J-PLUS data (both simulated and real galaxies) is out of the scope of this paper and will be presented in a future work. The CALIFA/STARLIGHT analysis does not provide direct error estimates in its output. Based on simulations by Cid Fernandes et al. (2014) and de Amorim et al. (2017), estimated uncertainties of physical quantities obtained by STARLIGHT are $\Delta \mathrm{Age}_M = 1.4$ Gyr, $\Delta [\mathrm{Fe/H}]_M = 0.12$ dex, and $\Delta A_v = 0.05$. These uncertainty estimates must be interpreted as approximate, as

they are based on experiments with a single galaxy, and do not take into consideration sources of error other than random noise.

4.2. Goodness-of-fit maps

Despite the general high quality data of CALIFA and J-PLUS, variations in data quality across the image of a given galaxy or from galaxy-to-galaxy can produce biased results. In addition, a poor fit can be produced even from good quality data (e.g., an unmasked emission line). Therefore, it is important to perform a quality control check of the data and the fit. Figures 5 and 6 show the different data and fit quality maps reported by J-PLUS/MUFFIT, CALIFA/STARLIGHT, and CALIFA/STECKMAP for NGC 5473 and NGC 5485, respectively.

The J-PLUS/MUFFIT map shows as quality indicators the bin-by-bin S/N in the filter $J0515$, the magnitude error of the $J0515$ filter, and the reduced χ^2 map of the SED fitting (first row of Figs. 5 and 6). The reference filter $J0515$ was chosen exclusively for comparison purposes with the CALIFA methods. Figures 5a and 6a show the CVT zones for the two galaxies color-coded by the S/N in the $J0515$ filter. As expected, the outer parts of the galaxies correspond to larger bins, while the bins associated with the central region are composed by single pixels. All the SEDs have $S/N > 20$ in the $J0515$ reference image. The χ^2 map of every object is inspected as a goodness-of-fit quality check (Figs. 5b and 6b). A detailed definition of the error-weighted χ^2 minimization process can be found in Sect. 3.2.1 of Díaz-García et al. (2015). Although generally speaking, a value of $\chi^2 \sim 1$ represents a good fit, the value of χ^2 should only be considered as an indicator because this value strongly depends on the photometric errors estimate. The χ^2 maps show small values in both cases. Visual inspection of the error maps (Figs. 5c and 6c) does not show evidence of significantly higher photometric errors that could suggest any artificial feature. Finally the distribution of the residuals of the best fitting are also examined. Figure 7 shows the distribution of the residuals for each filter. We note that while the red filters are always well fitted producing a small median residual and a small interquartile range (black symbols), the blue filters show a larger residual distribution. In particular, median residuals for filters J0395 and J0410 are ~0.1. This effect could be a consequence of the calibration technique performed since the zero point uncertainties of those filters are larger than in the rest of the filters. The J-PLUS calibration applies a series of calibration procedures rather than relying on a single calibration technique. While the photometric calibration in some filters is performed based on SDSS spectroscopic observations, photometric SDSS observations are used to calibrate the bands uncovered by SDSS spectra. The spectrophotometric standard star technique is critical in the calibration of the J0378 filter, since neither SDSS photometry nor SDSS spectroscopy cover this bandpass. Although this procedure has the advantage of providing an independent calibration for each filter, it is also possible to apply methods that enable us to anchor the calibration across the spectral range by combining the information from different bands.

A potential problem with the calibration of the J-PLUS blue filters could produce a bias in the final results. For this reason, the J-PLUS calibration and its implication need to be explored in detail. As described in J-PLUS Paper I, different calibration procedures are currently been tested. One particular promising approach is the use of the stellar locus (Covey et al. 2007; High et al. 2009; Kelly et al. 2014), which optimally suits
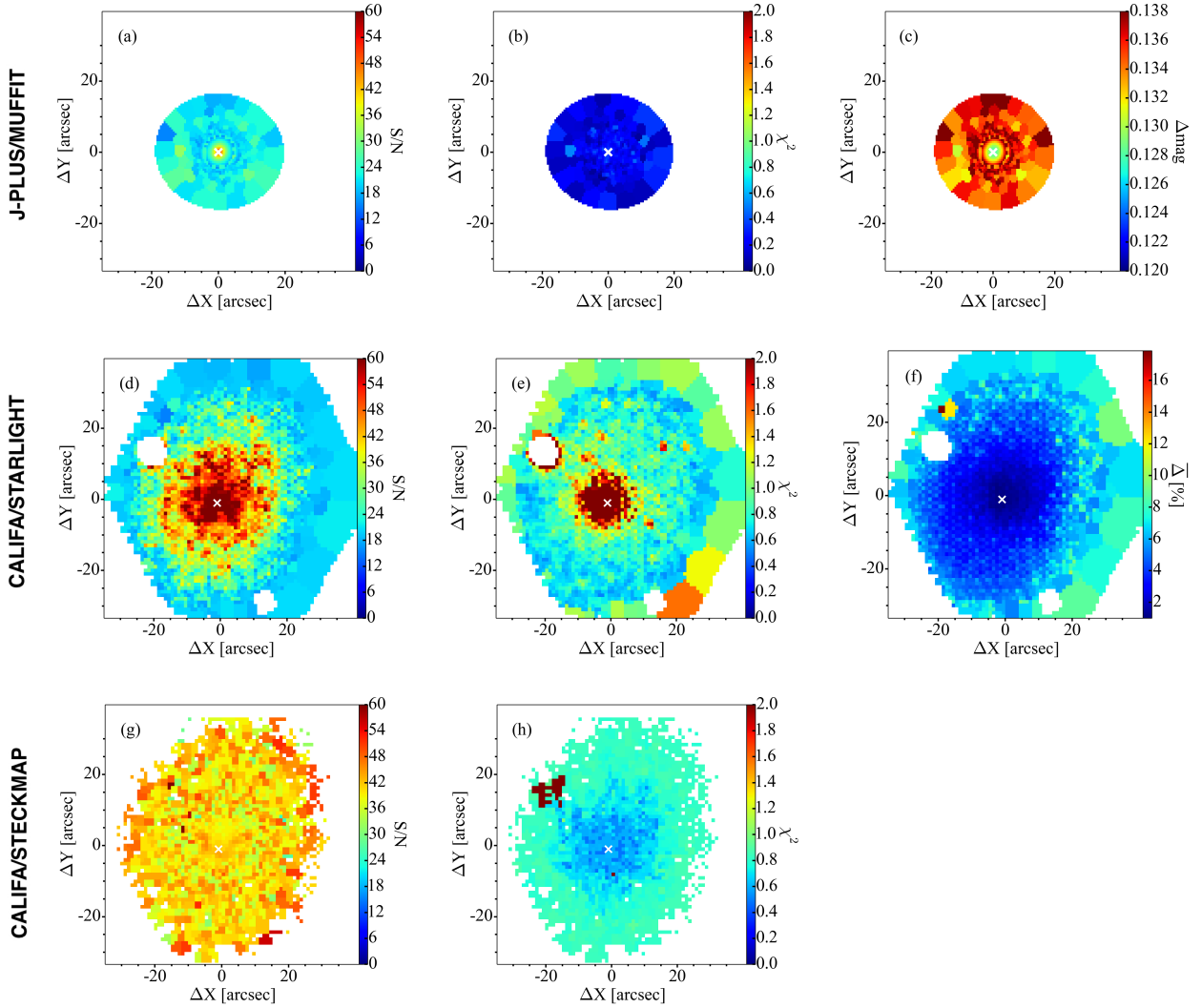
Fig. 5. Maps with data and fit quality indicators for NGC 5473 determined by J-PLUS/MUFFIT (*top panels*), CALIFA/STARLIGHT (*middle panels*), and CALIFA/STECKMAP (*bottom panels*). The center of the galaxy is indicated with a white cross in each panel.

systems with large fields of view such as in J-PLUS. This procedure profits from the way stars with different stellar parameters populate color-color diagrams, defining a well-limited region (stellar locus) whose shape depends on the specific colors used. A specific stellar locus approach for the calibration of J-PLUS has been developed, obtaining consistent zero point calibrations over the full J-PLUS spectral range. As preliminary results, Paper I presents the zero point calibration and their uncertainties for the J-PLUS data release 1 (DR1) using different procedures. A significant improvement in such zero point uncertainties is reported, in all cases ≤0.026 and as small as 0.010, demonstrating the power of the stellar locus to calibrate large photometric data sets. The details of this procedure and its application to J-PLUS data will be presented in a future work.

The second row in Figs. 5 and 6 shows quality indicator maps for CALIFA/STARLIGHT method. The spaxels with artifacts, foreground objects, and very low S/N (<3) are masked and appear as white regions in the maps. The spaxels with S/N lower than 20 in the 5635 ± 45 Å band are binned into Voronoi zones (e.g., two or more spaxels are contained in a given zone). As shown by Figs. 5d and 6d, only the very outer parts of each galaxy are affected by low S/N spaxels. After the Voronoi binning, all the spectra have $S/N > 20$ at 5635 Å. Figures 5e

and 6e present the reduced χ^2 for the CALIFA/STARLIGHT analysis. As discussed previously, χ^2 is closely tied to the uncertainty of the spectra, meaning that inspection of Figs. 5e and 6e may lead to the wrong conclusion that the fits are worse in the central regions than in the outskirts. Based on this argument, CALIFA/STARLIGHT also provides the mean absolute model deviation, $\overline{\Delta}$ maps (Figs. 5f and 6f). The value $\overline{\Delta}$ does not depend explicitly on the uncertainties so it is a more appropriate measure of the fit quality. A detailed definition of χ^2 and $\overline{\Delta}$ can be found in Cid Fernandes et al. (2013). As noted by Cid Fernandes et al. (2013), the inspection of the highest $\overline{\Delta}$ spectra often reveals nonmasked emission lines or artifacts. The median $\overline{\Delta}$ value for the ~10⁵ CALIFA analyzed spectra was 4% (corresponding to an equivalent S/N of 25), and in less than 2% of the cases $\overline{\Delta}$ exceeds 10%.

As explained in Sect. 3, the Voronoi tessellation is different for each method. Although ideally the same binning segmentation should be used for a fair comparison (i.e., same areas/spectra of the object are compared), in practice this is not convenient. Different observing conditions between J-PLUS and CALIFA would require degrading J-PLUS quality data to match CALIFA PSF and spatial resolution (e.g., strong homogenization of the data). Even when considering
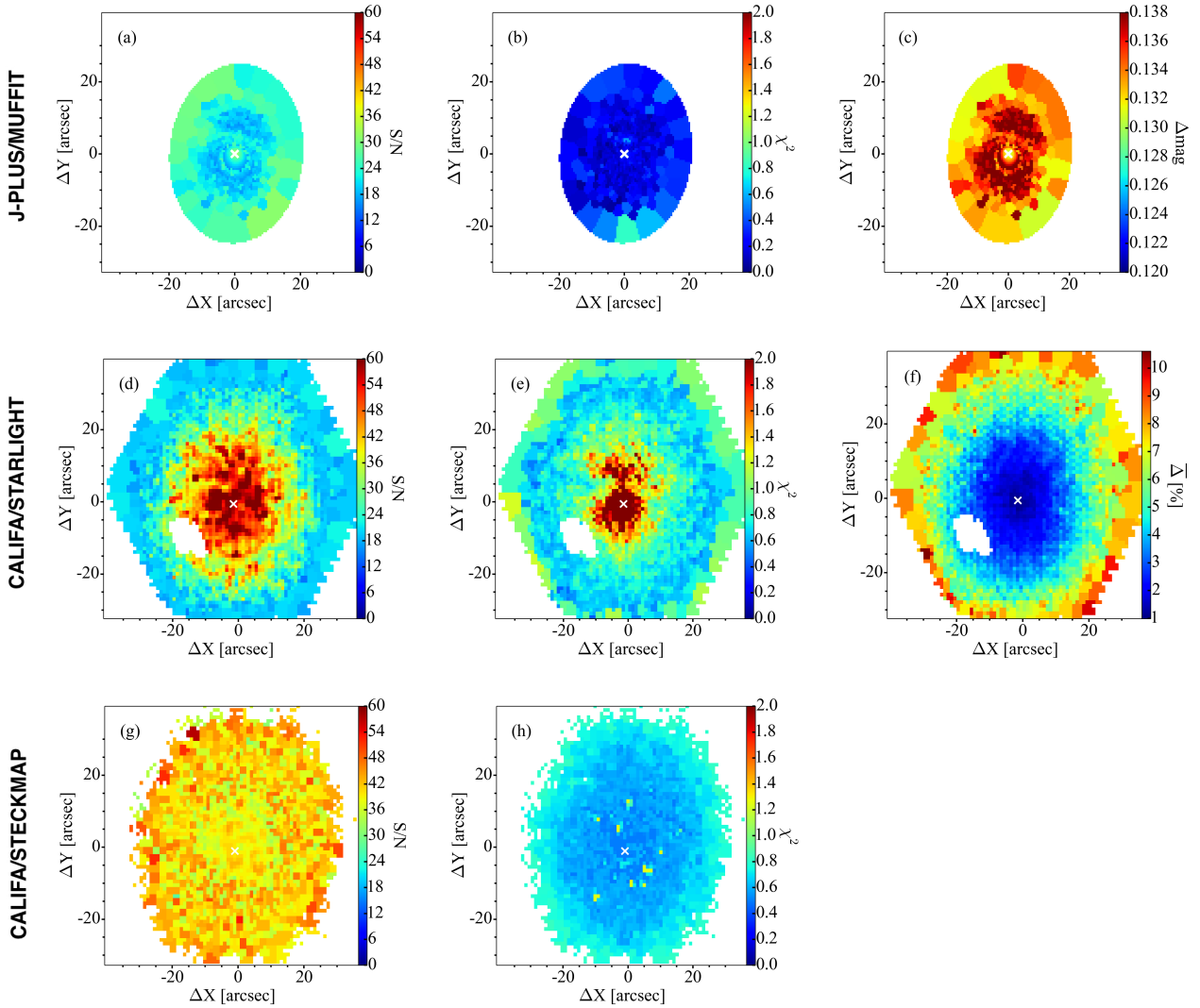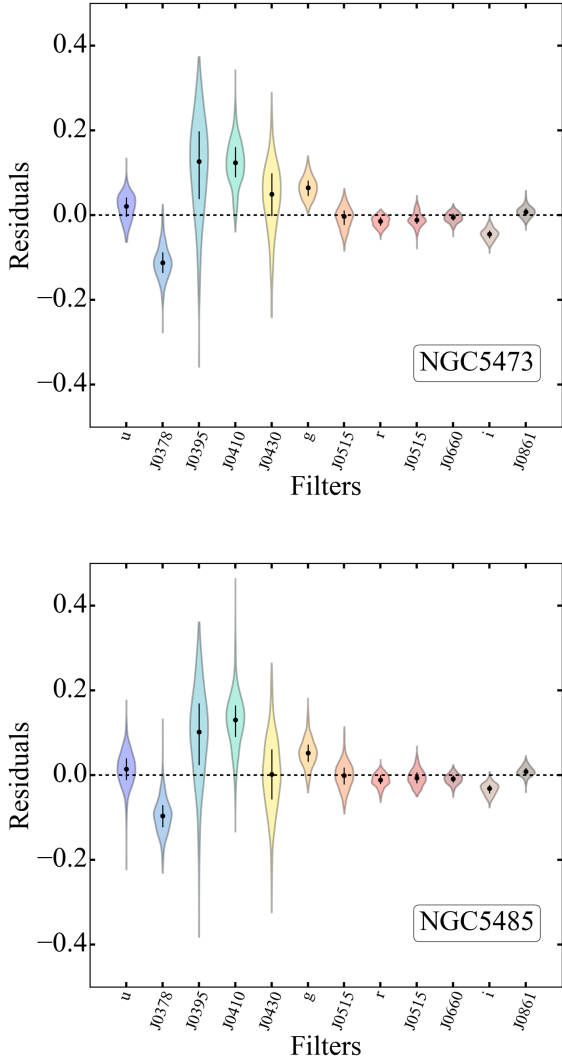
Fig. 6. Same as in Fig. 5, but for NGC 5485.

the same observing data (CALIFA/STARLIGHT and CAL-IFA/STECKMAP), the peculiarities of each method require a different treatment to ensure a reliable determination of the output parameters (e.g., different minimum S/N required). For these reasons, we applied each method under the best possible conditions and produce different S/N and binning maps (Figs. 5 and 6) from survey to survey (J-PLUS versus CAL-IFA) and also from technique to technique (STARLIGHT versus STECKMAP).

5. Radial profiles

To quantify radial variations of the galaxies properties, we present in Figs. 8 and 9 the mass- and luminosity-weighted radial profiles of the stellar population parameters. We obtained the J-PLUS/MUFFIT profiles following the technique described in San Roman et al. (2018). They have plotted the stellar properties values of each bin in each galaxy as a function of the circularized galactocentric distance, R' (see their Eq. (3)). The final profiles were obtained by averaging the stellar population properties of the sample in constant bins of $0.2\,R_{eff}$ for $0 \le R \le 3.5\,R_{eff}$. The errors correspond to the standard deviation of the mean in each bin. The CALIFA/STARLIGHT and CALIFA/STECKMAP profiles were derived by binning the output values into elliptical

annuli that are scaled in along the major axis such that the bins are constant in effective radius. Elliptical apertures of $0.1\,R_{eff}$ were used to extract the radial profiles. These azimuthally averaged radial profiles assume a priori symmetry in the stellar population of the galaxies by directly collapsing the information to a 1D plot. Same position angles, ellipticities, and R_{eff} were used to obtain J-PLUS/MUFFIT and CALIFA/STECKMAP profiles. Along the semimajor axis $R' = R$, so the profiles derived by the different techniques are directly comparable. Enclosed shadowed regions correspond to the uncertainties of each profile.

Figures 8 and 9 show an offset between the different methodologies with differences up to $\Delta\log\,\mathrm{Age} = 0.3\,\mathrm{dex}$ and $\Delta[\mathrm{Fe/H}] = 0.1\,\mathrm{dex}$. The existence of intrinsic systematic differences between the three methods seems to be the most plausible reason for the different absolute values of the derived stellar parameters. The discrepancies between the analysis of spectral features versus colors, together with the assumptions of different star formation histories may be responsible for the quantitative discrepancies. For each individual method, the age and metallicity radial profiles are very similar (i.e., same gradient) when luminosity- and mass-weighted properties are used. This result agrees with previous studies (San Roman et al. 2018; González Delgado et al. 2014), and confirms that the contribution of the second SSP (the younger component) is small and the

Fig. 7. Distribution of the residuals of the best fitting for each J-PLUS filter (enclosed colored regions). The black symbols and bars correspond to the medians and interquartile range for each distribution.
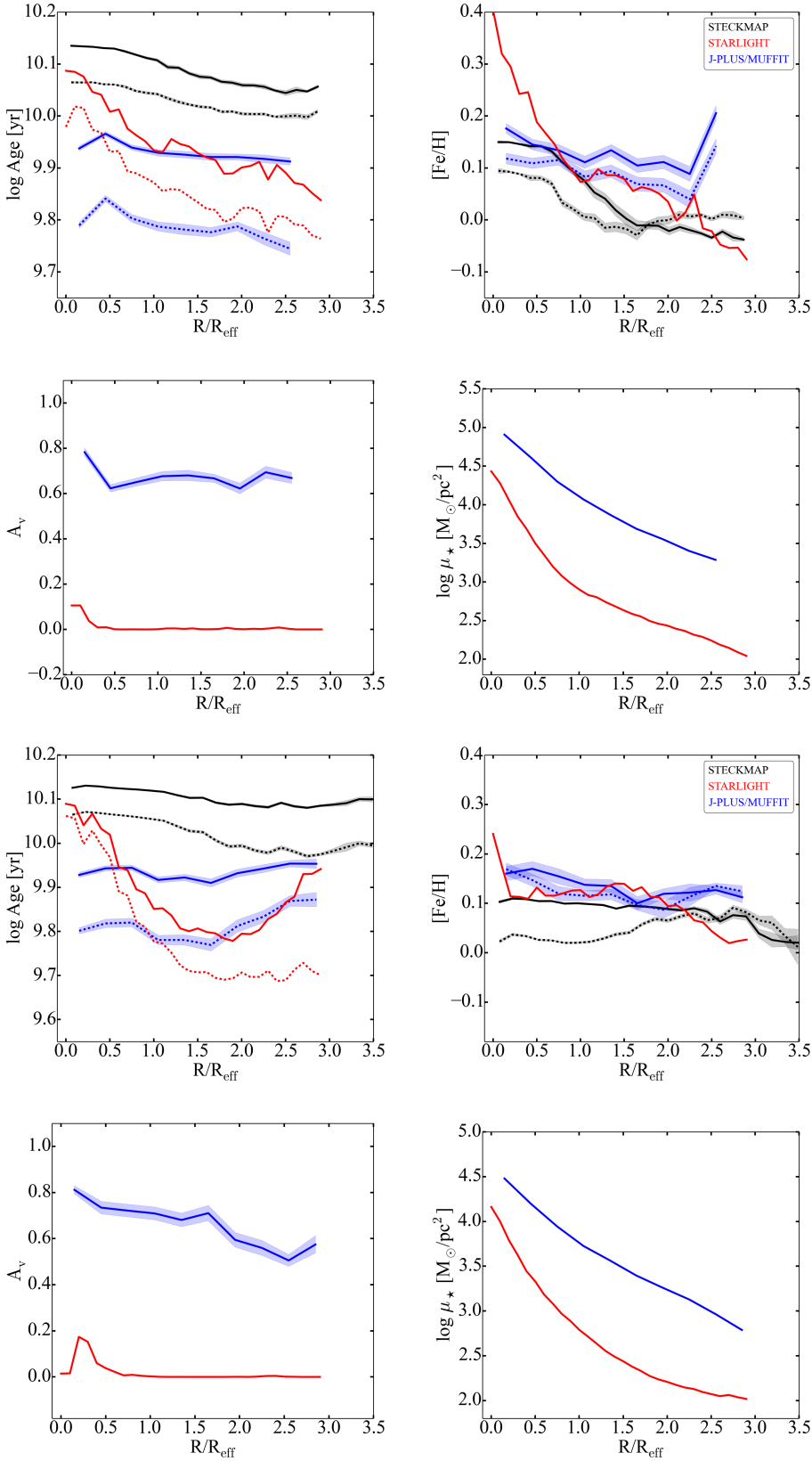
Table 3. Ages and metallicities values determined within different circular aperture using Lick index measurements (SSP) and mass-weighted parameters from spectral fitting (SFH) by the ATLAS[3D] survey.

R_{circ}	NGC 5473		NGC 5485	
	$\mathrm{Age_{SSP}}$ (Gyr)	$\mathrm{[Fe/H]_{SSP}}$	$\mathrm{Age_{SSP}}$ (Gyr)	$\mathrm{[Fe/H]_{SSP}}$
$R_{eff}/8$	6.87 ± 1.25	0.21 ± 0.05	9.69 ± 1.68	0.05 ± 0.05
$R_{eff}/2$	9.69 ± 1.68	-0.01 ± 0.05	11.51 ± 2.14	-0.12 ± 0.05
R_{eff}	11.51 ± 1.99	-0.14 ± 0.06	12.55 ± 2.28	-0.20 ± 0.05
	$\mathrm{Age_{SFH}}$ (Gyr)	$\mathrm{[Fe/H]_{SFH}}$	$\mathrm{Age_{SHF}}$ (Gyr)	$\mathrm{[Fe/H]_{SHF}}$
R_{eff}	11.63 ± 0.65	-0.10 ± 0.02	12.78 ± 0.75	-0.12 ± 0.02

ing no significant changes in the dust content. In contrast, CALIFA/STARLIGHT results show a dust-free content ($A_v = 0$) at $R > 0.5R_{eff}$ with inner regions showing $A_v < 0.2$ value for both galaxies. The stellar mass surface density profiles, $\log \mu_\star$, also show differences in the structures where J-PLUS/MUFFIT presents a more linear decline in the profiles. These differences in the stellar mass surface density may be a consequence of the large differences in the extinction parameter.

Overall, Figs. 8 and 9 show that the profiles obtained by J-PLUS/MUFFIT and CALIFA/STECKMAP present a linear behavior with the galactocentric distance (i.e., flat age gradient and negative metallicity gradient). On the contrary, CALIFA/STARLIGHT presents nonlinear profiles (i.e., negative gradients in the inner part of the galaxies ($<R_{eff}$) that flatten at larger galactocentric distances) producing different inner and outer gradients.

As mentioned previously, the ATLAS[3D] survey observed our two target objects using SAURON spectrograph. These IFU observations are limited by a small wavelength range (480–538 nm) and focused on the very center of the galaxies. They determined the stellar population content applying two methods: one based on measuring line-strength indices and applying SSP models to derive SSP-equivalent values; and another one based on spectral fitting to derive nonparametric star formation histories, mass-weighted average values of age, metallicity, and half-mass formation timescales. Using spectra integrated within three apertures covering up to one effective radius ($R_{eff}/8$, $R_{eff}/2$ and $1\,R_{eff}$), McDermid et al. (2015) obtained average values of age and metallicity based on measuring the Lick indices Hβ, Fe5015, Mgb, and Fe5270 (Worthey et al. 1994) and using SSP models. Age values inferred at various apertures showed that the young stars are more centrally concentrated implying positive age gradients. The derived metallicity becomes lower at larger apertures because of the inclusion of the metal-poor outer regions. To obtain the mass-weighted parameters from spectral fitting, they used the penalized pixel fitting code pPXF (Cappellari & Emsellem 2004) to fit a linear combination of SSP model spectra from the MIUS-CAT model library (Vazdekis et al. 2012). They fit the integrated spectra within one effective radius. We note that the ages and metallicities obtained by McDermid et al. (2015) are integrated aperture measurements and therefore are not directly comparable with the radial profiles presented in Figs. 8 and 9. The ages and values are presented in Table 3. The results of ATLAS[3D] for NGC 5485 would agree with the flat or slightly positive age gradient found by J-PLUS/MUFFIT and CALIFA/STECKMAP up to one effective radius, however they would contrast with the strong negative age gradient observed in CALIFA/STARLIGHT profile for the same area.

star formation history of early-type galaxies is well represented mainly by an old SSP component.

The radial profile shapes, however, show clear differences between the three methods. NGC 5473 (Fig. 8) shows flat or slightly negative age profiles in J-PLUS/MUFFIT and CALIFA/STECKMAP analysis, while the CALIFA/STARLIGHT age profile is significantly steeper. The metallicity profiles are negative in all the cases although the J-PLUS/MUFFIT metallicity gradient seems flatter than in the other two methods. In contrast, NGC 5485 profiles present significant differences from method to method, which are more clearly evident in the age profiles. While J-PLUS/MUFFIT and CALIFA/STECKMAP show similar flat age gradients, CALIFA/STARLIGHT presents a u-shaped $\log \mathrm{Age_M}$ profile with a strong negative age gradient inside $1.5\,R_{eff}$ that becomes positive at larger radii. The luminosity-weighted age profile, $\log \mathrm{Age_L}$, of STARLIGHT also presents significant differences with the other methods showing a strong negative inner ($<1.5R_{eff}$) gradient that flattens at larger radii. The slightly negative [Fe/H] profiles seem to be compatible between the different methods. Results of J-PLUS/MUFFIT of the stellar extinction behavior are consistent with a flat or slightly negative A_v profile with a constant $A_v \sim 0.7$ suggest-

Fig. 8. Mass-weighted (solid lines) and luminosity-weighted (dashed lines) radial profiles for NGC 5473 of log Age, [Fe/H], A_v, and log $\mu_\star$ for the three different methods. Enclosed shadowed regions correspond to the uncertainties of each profile.

Fig. 9. Same as in Fig. 8, but for NGC 5485.

6. Stellar mass-to-light ratio

Stellar masses play a crucial role in the study of galaxy properties and the evolution of the galaxy population. Even though it is generally accepted that the analysis of galaxies by their estimated stellar masses rather than observed luminosities provides a more physical insight, it is also recognized that we are limited by a number of statistical and systematic uncertainties when translating observational quantities into physical parameters. Besides the accuracy of the population synthesis models used to interpret observations (e.g., different stellar libraries

or particular stellar evolutionary phases), dust attenuation is a key uncertainty in stellar mass, $M_\star$, and mass-to-light ratio, $M_\star/L$, values. Although dust can also affect absorption features such as the 4000 Å-break (MacArthur 2005), this uncertainty is especially relevant when using color information in the analysis (e.g., Zibetti et al. 2009; Sorba & Sawicki 2015). If the attenuation is patchy, such as the case of NGC 5485, using spatially resolved $M_\star$ and $M_\star/L$ and then integrating the results galaxy-wide, reduces this systematic uncertainty (e.g., Zibetti et al. 2009; Sorba & Sawicki 2015).

Figure 10 shows the $M_\star/L$ maps derived with J-PLUS/ MUFFIT for NGC 5473 and NGC 5485. $M_\star/L$ ratios are derived considering the $J0515$ filter as the reference band. For the absolute magnitude of the Sun in the reference filter, we convolved J-PLUS $J0515$ filter with the solar spectrum. It can be seen that $M_\star/L$ is almost constant across both galaxies, although NGC 5485 presents a significant increase in $M_\star/L$ clearly associated with the minor-axis dust lane. Table 4 presents the log $M_\star^{\rm resolved}$ and $(M_\star/L)^{\rm resolved}$ obtained by integrating the spatially resolved maps.

7. Integrated properties

In addition to the spatially resolved stellar properties of each galaxy, we also determined the global stellar properties of the two galaxies. Table 4 summarizes the global properties of the two galaxies determined using the integrated photometry for J-PLUS/MUFFIT, and the integrated spectra for CALIFA/ STARLIGHT and CALIFA/STECKMAP.

Table 4 shows some discrepancies between the global properties of the galaxies analyzed by J-PLUS/MUFFIT, CALIFA/ STARLIGHT, and CALIFA/STECKMAP. Differences can reach up to $\Delta\log\,{\rm Age} = 0.1$ dex ($\Delta{\rm Age} \sim 2\,{\rm Gyr}$) and up to $\Delta{\rm Fe/H} = 0.1$ dex. Díaz-García et al. (2015), using results from MUFFIT, analyzed a subsample of red sequence galaxies shared by ALHAMBRA and SDSS. The one-to-one comparison between metallicities and ages derived spectroscopically for the SDSS data (Gallazzi et al. 2005) and those determined from MUFFIT and ALHAMBRA revealed good qualitative agreement but a systematic difference of $\sim 2\,{\rm Gyr}$ between the two methods. After an exhaustive investigation of the potential origin of the offset, they concluded that the existence of intrinsic systematic differences between the two methods seems to be the most plausible reason for the difference in the absolute values of the derived ages. The differences between the extinction parameters obtained by the different methods are even more significant.

To closely inspect any potential systematic effect between J-PLUS and CALIFA data, we directly compared the photo-spectra analyzed by J-PLUS and the integrated spectra of CALIFA. Figure 11 shows the comparison between the integrated spectra in a $3''$ diameter fiber of SDSS, CALIFA and the photo-spectrum of J-PLUS for NGC 5485. The spectra are normalized to the r band. We note that SDSS does not provide the NGC 5473 spectrum so the analogous comparison for this object cannot be shown. We also note that the apertures used are not exactly equivalent. The CALIFA extraction is made in a $3'' \times 3''$ area centered in the continuum peak of the V500 spectral setup while the integrated J-PLUS photo-spectrum is obtained using a circular aperture of $3''$ diameter. In addition, the precise position of the SDSS fiber is unknown, thereby producing potential differences in the aperture centering. In spite of these differences both observations closely follow the SDSS spectrum. This is not surprising since the calibration of J-PLUS and CALIFA observations are anchored to SDSS. In
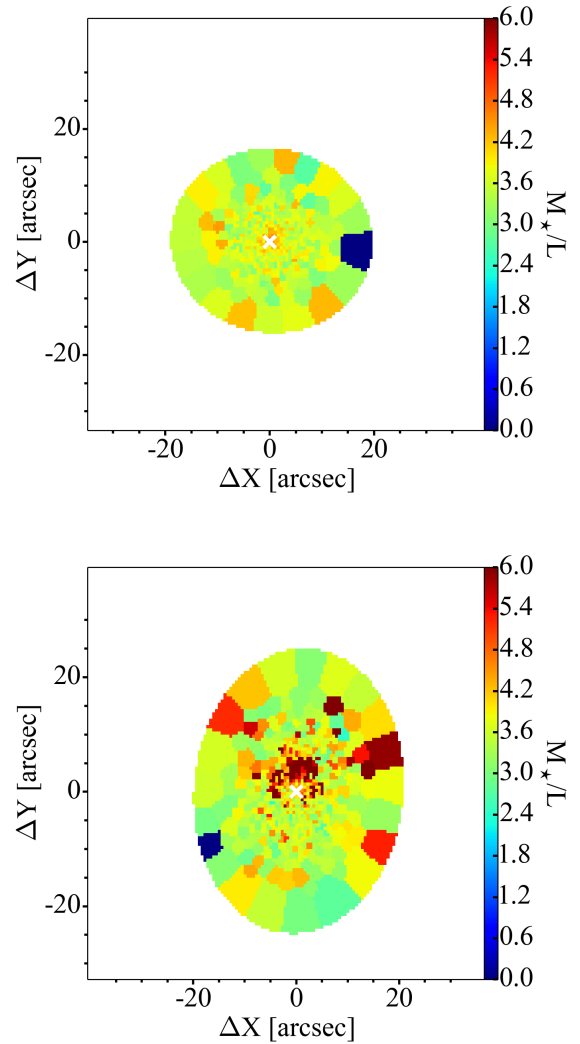
Fig. 10. Stellar mass-to-light ratio maps determined by J-PLUS/ MUFFIT for NGC 5473 (*top panel*) and NGC 5485 (*bottom panel*). The center of the galaxy is indicated with a white cross in each panel.

order to ultimately compare the three methods, we performed the analysis on these spectra/pseudo-spectra where the spectra and the photometry concur. Figure 11 shows the best-fitting model to the photo-spectrum of J-PLUS as green circles where the bottom panel shows the residuals of this best-fitting model. As discussed in Sect. 4.2, we considered several approaches to improve the discrepancies and potential problems of J-PLUS data at blue wavelengths and these will be presented in a future work. The properties of the best-fitting models obtained using the three different methods are collected in Table 5. Table 5 shows the results of J-PLUS/MUFFIT on the $3''$ integrated photometry, and the results of CALIFA/STARLIGHT and CALIFA/STECKMAP on the same $3'' \times 3''$ integrated spectra. Overall, differences reach up to $\Delta\log\,{\rm Age} = 0.2$ dex ($\Delta{\rm Age} \sim 3.5\,{\rm Gyr}$) and up to $\Delta{\rm Fe/H} = 0.2$ dex. Once again, the differences between the extinction parameters obtained by J-PLUS/MUFFIT and CALIFA/ STARLIGHT are very large. The assumption of different star formation histories or the different spectral range covered by CALIFA and J-PLUS may be responsible for the quantitative discrepancies. The differences between CALIFA/STARLIGHT and CALIFA/STECKMAP are more remarkable. Even when the same spectra and very similar stellar population models are used (see Sect. 3) discrepancies are significant, reaching
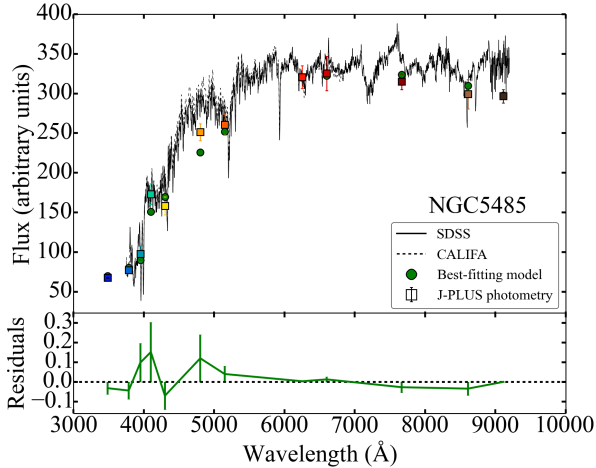
Fig. 11. Comparison between the integrated spectra in a 3″ diameter fiber of SDSS, CALIFA, and the photo-spectrum of J-PLUS for NGC 5485. Error bars correspond to the photometric errors. The best-fitting model to the photo-spectrum of J-PLUS is plotted as green circles. *Bottom panel*: residuals of the best-fitting model.

$\Delta \log\ \mathrm{Age_M} = 0.12\,$dex (i.e., $\Delta \mathrm{Age_M} = 3\,$Gyr) and $\Delta \mathrm{Fe/H_M} = 0.27\,$dex. This comparison must be interpreted with caution as it is based on one single spectra. Future work is required to evaluate in detail the origin of these differences and to clearly quantify them.

8. Discussion

Early-type galaxies were once considered uniform stellar systems with little gas, dust, and nuclear activity. We now know that early-type galaxies commonly contain a large amount of dust in either organized or complex structures (e.g., Sadler & Gerhard 1985; van Dokkum & Franx 1995; Tran et al. 2001). In a fraction of the early-type galaxy population, the dust is organized in prominent and large-scale dust lanes. These so-called dust-lane early-type galaxies are considered to be the remnants of recent gas-rich minor mergers with a low star formation efficiency (Hawarden et al. 1981; Kaviraj et al. 2012; Shabala et al. 2012; Davis et al. 2015). If we assume that dust and gas settle in the principal planes of a galaxy, the existence of a minor axis dust lane in NGC 5485 is a visual evidence for its triaxiality. This triaxiality is also supported by its rather exceptional kinematical structure, which shows strong minor-axis rotation known as prolate rotation (Wagner et al. 1988; Krajnović et al. 2011; Emsellem et al. 2011; Tsatsi et al. 2017).

Baes et al. (2014) pointed out that despite a noticeable amount of dust, neither neutral nor molecular hydrogen has been detected in NGC 5485. This anomaly produces an extremely low gas-to-dust ratio, which is almost an order of magnitude lower than the canonical value for the Milky Way. Baes et al. (2014) proposed a potential scenario in which NGC 5485 would be recently merged with an SMC-type metal-poor galaxy where a substantial fraction of the HI could have been lost during the interactions. Using IFU CALIFA data and studying N-body merger simulations, Tsatsi et al. (2017) proposed a different formation scenario. They found that a prolate early-type galaxy, such as NGC 5485, may have been formed by a gas-poor, polar major merger that happened 10 Gyr ago. The galaxy was imaged in Hα by Finkelman et al. (2010) who detected an ionized gas disk that closely follows the dust structure. These authors found that the Hα emission and color of

NGC 5485 is consistent with the presence of an old stellar population (~4.5 Gyr) and a small fraction of a young population (~10–350 Myr). The nature of the ionized gas emission found in early-type galaxies is still under debate since nonstellar ionization mechanisms (e.g., induced shocks), stellar ionization mechanisms (e.g., low level of star formation, post-AGB) or even AGN effects may contribute to the excitation of the warm ionized medium (e.g., Dopita & Sutherland 1995; Stasińska et al. 2008; Papaderos et al. 2013).

As shown in Fig. 3, the age maps of NGC 5485 present significant differences between the three methods. If the old stellar component, aligned with the dust lane, present in the CALIFA/STARLIGHT maps is a real feature, the stellar component could be associated with the NGC 5485 kinematic structure and would favor the polar major merger scenario at 10 Gyr. This interpretation would not however explain the absence of the aligned old stellar component in the CALIFA/STECKMAP and J-PLUS/MUFFIT maps. It would also contrast the centrally concentrated young stars found by ATLAS[3D]. On the other hand, if the position, size, and orientation of the old component in the CALIFA/STARLIGHT is an artificial feature, this suggests that a potential age-extinction degeneracy could be affecting the results. This means that a stellar population reddened by the old content can mimic the behavior of a population that has been reddened by extinction.

Overall, MaNGA early-type galaxies exhibit relatively flat radial profiles with reddening values between $E(B-V) \sim 0.06$, which corresponds[7] to $A_v \sim 0.2$. However, higher values of $E(B-V) = 0.25$ corresponding to $A_v = 0.8$ are not unusual in dusty early-type galaxies (Goddard et al. 2017; Wilkinson et al. 2015). Unfortunately, the lack of previous extinction values studies of NGC 5485 does not allow for further comparison.

Although the peculiarities of NGC 5485 imposes an additional challenge to the comparison between the methods, the more standard case of NGC 5473[8] (i.e., absence of a dusty structure) reveals that the main source of discrepancies is due to the actual methods and not the singularities of the objects.

In addition, IFU MaNGA studies show discrepant conclusions when analyzing the same galaxy sample but using different spectral fitting techniques. Goddard et al. (2017), using the full spectral fitting code FIREFLY (Wilkinson et al. 2015, 2017) and the spectral population models of Maraston & Strömbäck (2011), found flat luminosity-weighted age gradients inside $R < R_{\rm eff}$. On the contrary, studying the same data set but using the full spectral fitting code STARLIGHT and BC03 models, Zheng et al. (2017) found a slightly negative gradient (–0.05 dex/$R_{\rm eff}$) at the same galactocentric distances. Goddard et al. (2017) performed a comparison between fitting codes and stellar population models. They concluded that overall, the luminosity-weighted ages are affected by systematic offsets between the various codes and underlying stellar population models on the order of –0.13 dex with a large scatter of 0.37 dex. The comparison for the luminosity-weighted metallicity is even more complex showing an overall difference of –0.24 dex with a large scatter of 0.34 dex. The choice of fitting technique also yields significant effects when the dependence of the stellar population models is isolated (i.e., same stellar

---

[7] Considering $R_v = A_v/E(B-V)$ and assuming a value of $R_v = 3.1$.

[8] We note that although visual inspection reveals no photometric peculiarities suggesting that NGC 5473 is an elliptical galaxy, the morpho-kinematic study of Méndez-Abreu et al. (2018) suggests that NGC 5473 is a S0 galaxy.

Table 4. Global stellar population properties of the galaxies using the integrated photometry/spectra.

NGC 5473	$\log \text{Age}_L$ (dex)	$\log \text{Age}_M$ (dex)	$[\text{Fe/H}]_L$ (dex)	$[\text{Fe/H}]_M$ (dex)	A_v (mag)	$\log M_\star$ ($M_\odot$)
J-PLUS/MUFFIT	9.92 ± 0.15	10.06 ± 0.08	0.17 ± 0.23	0.12 ± 0.26	0.43 ± 0.37	10.81
CALIFA/STARLIGHT	9.89	9.97	0.08	0.16	0.0	10.62
CALIFA/STECKMAP	9.83 ± 0.01	9.99 ± 0.01	-0.01 ± 0.01	-0.08 ± 0.01	...	...
NGC 5485	$\log \text{Age}_L$ (dex)	$\log \text{Age}_M$ (dex)	$[\text{Fe/H}]_L$ (dex)	$[\text{Fe/H}]_M$ (dex)	A_v (mag)	$\log M_\star$ ($M_\odot$)
J-PLUS/MUFFIT	9.93 ± 0.18	10.02 ± 0.14	0.25 ± 0.24	0.28 ± 0.21	0.34 ± 0.43	10.80
CALIFA/STARLIGHT	9.85	9.92	0.05	0.12	0.0	10.49
CALIFA/STECKMAP	9.88 ± 0.01	9.92 ± 0.01	0.04 ± 0.01	-0.01 ± 0.01	...	...

Table 5. Global stellar population properties of the galaxies using the integrated photometry/spectra in a 3″ aperture.

NGC 5485	$\log \text{Age}_L$ (Gyr)	$\log \text{Age}_M$ (Gyr)	$[\text{Fe/H}]_L$ (dex)	$[\text{Fe/H}]_M$ (dex)	A_v (mag)
J-PLUS/MUFFIT	9.76 ± 0.26	9.89 ± 0.18	0.12 ± 0.37	0.16 ± 0.37	0.91 ± 0.70
CALIFA/STARLIGHT	9.96	10.09	0.40	0.30	0.0
CALIFA/STECKMAP	9.87 ± 0.05	9.97 ± 0.05	0.13 ± 0.02	0.21 ± 0.03	...

population models are used); this technique produces age offsets of -0.04 ± 0.45 dex and metallicity offsets of -0.11 ± 0.37 dex. A fundamental difference between both techniques is the treatment of dust: while STARLIGHT assumes a dust reddening law, FIREFLY is parameter free because it does not fit the continuum shape to constrain the stellar population properties. Differences in the extinction treatment method of our study are also present (Sect. 3).

The age and metallicity measurements are considerably affected by systematic differences, not only because of the stellar population models used, but also based on the fitting technique chosen. As a consequence, measurements of quantities such as age gradients are affected by uncertainties of similar magnitude as the signal itself. This problem clearly requires further investigation to include other spectral fitting codes. Future work is required to evaluate in detail the origin of these differences and explore possible paths to mitigate them.

9. Summary and conclusions

We illustrate the scientific potential of J-PLUS data to explore the spatially resolved stellar populations of local galaxies using a method that combines a CVT and MUFFIT multifilter SED fitting method. This technique allows us to analyze unresolved stellar populations of spatially resolved galaxies based on multifilter photometry. We present detailed 2D maps of stellar population properties (age, metallicity, extinction, and stellar mass surface density) for two early-type galaxies: NGC 5473 and NGC 5485. Radial structures were also obtained and luminosity- and mass-weighted profiles were derived out to $R = 3\,R_{\text{eff}}$. We compared J-PLUS/MUFFIT results with analysis from IFU CALIFA data for the same galaxies. Two different techniques to analyze IFU CALIFA were used: STARLIGHT and STECKMAP. We demonstrate that our alternative technique derives radial stellar population gradients in greater agreement with IFU technique such as CALIFA/STECKMAP but differs when CALIFA/STARLIGHT method is used.

A comparison of the absolute values reveals the existence of intrinsic systematic differences between the three methods. Dif-

ferences are also found in the 2D maps. While NGC 5473 shows flat age and slightly negative metallicity profiles, NGC 5485 age and extinction profiles are more challenging. The CALIFA/STARLIGHT method shows an older component in the center of the galaxy not present in the J-PLUS/MUFFIT and CALIFA/STECKMAP analyses. This older component has the same position, size, and orientation as the prominent dust line visible along the minor-axis of the galaxy. Although CALIFA/STARLIGHT detects the dust feature in the A_v map, values are significantly lower than those obtained by J-PLUS/MUFFIT. Radial profile shape of NGC 5485 also presents a different behavior between different methods. The CALIFA/STARLIGHT method presents a u-shaped age profile with strong negative age gradient inside $1.5\,R_{\text{eff}}$ that become positive at larger radii while a flat age gradient is present in the J-PLUS/MUFFIT and CALIFA/STECKMAP analyses.

For each methodology, the age and metallicity radial profiles are very similar when luminosity- or mass-weighted properties are used, suggesting that the mass assembly of the early-type galaxies NGC 5473 and NGC 5485 are followed by their luminosity components.

Although discrepancies between the analysis of spectral features and colors together with different star formation histories assumptions and the different spectral range may be responsible for the discrepancies between J-PLUS/MUFFIT and CALIFA/STECKMAP, significant offsets are also present when similar analysis conditions are present (e.g., CALIFA/STARLIGHT versus CALIFA/STECKMAP). This result suggests that the specific characteristics of each method such as the extinction treatment used may cause important differences. We conclude that the ages, metallicities, and extinction derived for individual galaxies not only depend on the chosen models but also depend on the method used. This problem clearly requires further investigation to evaluate in detail the origin of these differences.

Finally, we remark that although detailed investigations will require larger data sets, it is clear that photometric surveys such as the current J-PLUS (Paper I) and the upcoming J-PAS (Benitez et al. 2014) will extend 2D multifilter studies such as that presented in this work to scientific cases not available to

References

Astropy Collaboration (Robitaille, T. P., et al.) 2013, A&A, 558, A33
Baes, M., Allaert, F., Sarzi, M., et al. 2014, MNRAS, 444, L90
Benitez, N., Dupke, R., Moles, M., et al. 2014, ArXiv e-prints [arXiv:1403.5237]
Bershady, M. A., Verheijen, M. A. W., Swaters, R. A., et al. 2010, ApJ, 716, 198
Bertin, E. 2006, in Astronomical Data Analysis Software and Systems XV, eds. C. Gabriel, C. Arviset, D. Ponz, & S. Enrique, ASP Conf. Ser., 351, 112
Bertin, E. 2011, in Astronomical Data Analysis Software and Systems XX, eds. I. N. Evans, A. Accomazzi, D. J. Mink, & A. H. Rots, ASP Conf. Ser., 442, 435
Bertin, E. 2013, Astrophysics Source Code Library [record ascl:1301.001]
Bertin, E., & Arnouts, S. 1996, A&AS, 117, 393
Bertin, E., Mellier, Y., Radovich, M., et al. 2002, in Astronomical Data Analysis Software and Systems XI, eds. D. A. Bohlender, D. Durand, & T. H. Handley, ASP Conf. Ser., 281, 228
Blanc, G. A., Gebhardt, K., Heiderman, A., et al. 2010, in New Horizons in Astronomy: Frank N. Bash Symposium 2009, eds. L. M. Stanford, J. D. Green, L. Hao, & Y. Mao, ASP Conf. Ser., 432, 180
Boardman, N. F., Weijmans, A.-M., van den Bosch, R., et al. 2017, MNRAS, 471, 4005
Bonatto, C., Chies-Santos, A. L., Coelho, P. R. T., & J-PLUS collaboration 2019, A&A, 622, A179
Bressan, A., Fagotto, F., Bertelli, G., & Chiosi, C. 1993, A&AS, 100, 647
Bruzual, A. G. 2007, in Stellar Populations as Building Blocks of Galaxies, eds. A. Vazdekis, & R. Peletier, IAU Symp., 241, 125
Bruzual, G., & Charlot, S. 2003, MNRAS, 344, 1000
Bundy, K., Bershady, M. A., Law, D. R., et al. 2015, ApJ, 798, 7
Burstein, D., Faber, S. M., Gaskell, C. M., & Krumm, N. 1984, ApJ, 287, 586
Cappellari, M., & Copin, Y. 2003, MNRAS, 342, 345
Cappellari, M., & Emsellem, E. 2004, PASP, 116, 138
Cappellari, M., Emsellem, E., Krajnović, D., et al. 2011, MNRAS, 413, 813
Cappellari, M., Scott, N., Alatalo, K., et al. 2013, MNRAS, 432, 1709
Cardelli, J. A., Clayton, G. C., & Mathis, J. S. 1989, ApJ, 345, 245
Castander, F. J., Ballester, O., Bauer, A., et al. 2012, in Ground-based and Airborne Instrumentation for Astronomy IV, Proc. SPIE, 8446, 84466D
Cenarro, A. J., Moles, M., Cristóbal-Hornillos, D., & J-PLUS collaboration 2019, A&A, 622, A176
Chabrier, G. 2003, PASP, 115, 763
Cid Fernandes, R., Mateus, A., Sodré, L., Stasińska, G., & Gomes, J. M. 2005, MNRAS, 358, 363
Cid Fernandes, R., Pérez, E., García Benito, R., et al. 2013, A&A, 557, A86
Cid Fernandes, R., González Delgado, R. M., García Benito, R., et al. 2014, A&A, 561, A130
Coelho, P., Mendes de Oliveira, C., & Cid Fernandes, R. 2009, MNRAS, 396, 624
Colless, M., Dalton, G., Maddox, S., et al. 2001, MNRAS, 328, 1039
Cook, B. A., Conroy, C., Pillepich, A., Rodriguez-Gomez, V., & Hernquist, L. 2016, ApJ, 833, 158
Covey, K. R., Ivezić, Ž., Schlegel, D., et al. 2007, AJ, 134, 2398
Croom, S. M., Lawrence, J. S., Bland-Hawthorn, J., et al. 2012, MNRAS, 421, 872
Davis, T. A., Rowlands, K., Allison, J. R., et al. 2015, MNRAS, 449, 3503
de Amorim, A. L., García-Benito, R., Cid Fernandes, R., et al. 2017, MNRAS, 471, 3727
de Zeeuw, P. T., Bureau, M., Emsellem, E., et al. 2002, MNRAS, 329, 513
Dias, B., Coelho, P., Barbuy, B., Kerber, L., & Idiart, T. 2010, A&A, 520, A85
Díaz-García, L. A., Cenarro, A. J., López-Sanjuan, C., et al. 2015, A&A, 582, A14
Dopita, M. A., & Sutherland, R. S. 1995, ApJ, 455, 468
Driver, S. P., Hill, D. T., Kelvin, L. S., et al. 2011, MNRAS, 413, 971
Emsellem, E., Cappellari, M., Krajnović, D., et al. 2011, MNRAS, 414, 888
Fagotto, F., Bressan, A., Bertelli, G., & Chiosi, C. 1994a, A&AS, 104, 365
Fagotto, F., Bressan, A., Bertelli, G., & Chiosi, C. 1994b, A&AS, 105, 29
Ferreras, I., & Silk, J. 2000, ApJ, 541, L37
Finkelman, I., Brosch, N., Funes, J. G., Kniazev, A. Y., & Väisänen, P. 2010, MNRAS, 407, 2475
Fitzpatrick, E. L. 1999, PASP, 111, 63
Gallazzi, A., Charlot, S., Brinchmann, J., White, S. D. M., & Tremonti, C. A. 2005, MNRAS, 362, 41
Girardi, L., Bressan, A., Chiosi, C., Bertelli, G., & Nasi, E. 1996, A&AS, 117, 113
Goddard, D., Thomas, D., Maraston, C., et al. 2017, MNRAS, 466, 4731
González Delgado, R. M., Cerviño, M., Martins, L. P., Leitherer, C., & Hauschildt, P. H. 2005, MNRAS, 357, 945
González Delgado, R. M., Pérez, E., Cid Fernandes, R., et al. 2014, A&A, 562, A47
González Delgado, R. M., García-Benito, R., Pérez, E., et al. 2015, A&A, 581, A103
Hawarden, T. G., Longmore, A. J., Tritton, S. B., Elson, R. A. W., & Corwin, Jr., H. G. 1981, MNRAS, 196, 747
High, F. W., Stubbs, C. W., Rest, A., Stalder, B., & Challis, P. 2009, AJ, 138, 110
Hunter, J. D. 2007, Comput. Sci. Eng., 9, 90
Jones, E., Oliphant, T., Peterson, P., et al. 2001, SciPy: Open Source Scientific Tools for Python
Kaviraj, S., Schawinski, K., Devriendt, J. E. G., et al. 2007, ApJS, 173, 619
Kaviraj, S., Ting, Y.-S., Bureau, M., et al. 2012, MNRAS, 423, 49
Kelly, P. L., von der Linden, A., Applegate, D. E., et al. 2014, MNRAS, 439, 28
Krajnović, D., Emsellem, E., Cappellari, M., et al. 2011, MNRAS, 414, 2923
Kuntschner, H., Emsellem, E., Bacon, R., et al. 2010, MNRAS, 408, 97
Labbé, I., Franx, M., Rudnick, G., et al. 2003, AJ, 125, 1107
Le Borgne, J.-F., Bruzual, G., Pelló, R., et al. 2003, A&A, 402, 433
Logroño-García, R., Vilella-Rojo, G., López-Sanjuan, C., & J-PLUS collaboration 2019, A&A, 622, A180
Lonoce, I., Longhetti, M., Saracco, P., Gargiulo, A., & Tamburri, S. 2014, MNRAS, 444, 2048
López-Corredoira, M., Vazdekis, A., Gutiérrez, C. M., & Castro-Rodríguez, N. 2017, A&A, 600, A91
López-Sanjuan, C., Vázquez Ramió, H., Varela, J., & J-PLUS collaboration 2019, A&A, 622, A177
MacArthur, L. A. 2005, ApJ, 623, 795
Maraston, C., & Strömbäck, G. 2011, MNRAS, 418, 2785
Maraston, C., Daddi, E., Renzini, A., et al. 2006, ApJ, 652, 85
Marigo, P., & Girardi, L. 2007, A&A, 469, 239
Martín-Navarro, I., Vazdekis, A., Falcón-Barroso, J., et al. 2018, MNRAS, 475, 3700
Martins, L. P., González Delgado, R. M., Leitherer, C., Cerviño, M., & Hauschildt, P. 2005, MNRAS, 358, 49
McDermid, R. M., Alatalo, K., Blitz, L., et al. 2015, MNRAS, 448, 3484
Mehlert, D., Thomas, D., Saglia, R. P., Bender, R., & Wegner, G. 2003, A&A, 407, 423
Méndez-Abreu, J., Aguerri, J. A. L., Falcón-Barroso, J., et al. 2018, MNRAS, 474, 1307
Moles, M., Benítez, N., Aguerri, J. A. L., et al. 2008, AJ, 136, 1325
Molino, A., Benítez, N., Moles, M., et al. 2014, MNRAS, 441, 2891
Molino, A., Costa-Duarte, M. V., Mendes de Oliveira, C., & J-PLUS collaboration 2019, A&A, 622, A178
Ocvirk, P., Pichon, C., Lançon, A., & Thiébaut, E. 2006a, MNRAS, 365, 74
Ocvirk, P., Pichon, C., Lançon, A., & Thiébaut, E. 2006b, MNRAS, 365, 46
Papaderos, P., Gomes, J. M., Vílchez, J. M., et al. 2013, A&A, 555, L1
Pérez, F., & Granger, B. E. 2007, Comput. Sci. Eng., 9, 21
Pérez, E., Cid Fernandes, R., González Delgado, R. M., et al. 2013, ApJ, 764, L1
Pérez-González, P. G., Cava, A., Barro, G., et al. 2013, ApJ, 762, 46
Rawle, T. D., Smith, R. J., Lucey, J. R., & Swinbank, A. M. 2008, MNRAS, 389, 1891
Rawle, T. D., Smith, R. J., & Lucey, J. R. 2010, MNRAS, 401, 852

Reda, F. M., Proctor, R. N., Forbes, D. A., Hau, G. K. T., & Larsen, S. S. 2007, MNRAS, 377, 1772

Röck, B., Vazdekis, A., Ricciardelli, E., et al. 2016, A&A, 589, A73

Rogers, B., Ferreras, I., Peletier, R., & Silk, J. 2010, MNRAS, 402, 447

Rosales-Ortega, F. F., Kennicutt, R. C., Sánchez, S. F., et al. 2010, MNRAS, 405, 735

Roth, M. M., Kelz, A., Fechner, T., et al. 2005, PASP, 117, 620

Sadler, E. M., & Gerhard, O. E. 1985, MNRAS, 214, 177

San Roman, I., Cenarro, A. J., Díaz-García, L. A., et al. 2018, A&A, 609, A20

Sánchez, S. F., Kennicutt, R. C., Gil de Paz, A., et al. 2012, A&A, 538, A8

Sánchez, S. F., Rosales-Ortega, F. F., Iglesias-Páramo, J., et al. 2014, A&A, 563, A49

Sánchez, S. F., García-Benito, R., Zibetti, S., et al. 2016, A&A, 594, A36

Sánchez-Blázquez, P., Peletier, R. F., Jiménez-Vicente, J., et al. 2006, MNRAS, 371, 703

Sánchez-Blázquez, P., Forbes, D. A., Strader, J., Brodie, J., & Proctor, R. 2007, MNRAS, 377, 759

Sánchez-Blázquez, P., Ocvirk, P., Gibson, B. K., Pérez, I., & Peletier, R. F. 2011, MNRAS, 415, 709

Sánchez-Blázquez, P., Rosales-Ortega, F. F., Méndez-Abreu, J., et al. 2014, A&A, 570, A6

Sarzi, M., Falcón-Barroso, J., Davies, R. L., et al. 2006, MNRAS, 366, 1151

Shabala, S. S., Ting, Y.-S., Kaviraj, S., et al. 2012, MNRAS, 423, 59

Sorba, R., & Sawicki, M. 2015, MNRAS, 452, 235

Spolaor, M., Kobayashi, C., Forbes, D. A., Couch, W. J., & Hau, G. K. T. 2010, MNRAS, 408, 272

Stasińska, G., Vale Asari, N., Cid Fernandes, R., et al. 2008, MNRAS, 391, L29

Tran, H. D., Tsvetanov, Z., Ford, H. C., et al. 2001, AJ, 121, 2928

Tsatsi, A., Lyubenova, M., van de Ven, G., et al. 2017, A&A, 606, A62

van der Walt, S., Colbert, S. C., & Varoquaux, G. 2011, Comput. Sci. Eng., 13, 22

van Dokkum, P. G., & Franx, M. 1995, AJ, 110, 2027

Vazdekis, A., Ricciardelli, E., Cenarro, A. J., et al. 2012, MNRAS, 424, 157

Verheijen, M. A. W., Bershady, M. A., Andersen, D. R., et al. 2004, Astron. Nachr., 325, 151

Wagner, S. J., Bender, R., & Moellenhoff, C. 1988, A&A, 195, L5

Wilkinson, D. M., Maraston, C., Thomas, D., et al. 2015, MNRAS, 449, 328

Wilkinson, D. M., Maraston, C., Goddard, D., Thomas, D., & Parikh, T. 2017, MNRAS, 472, 4297

Wolf, C., Meisenheimer, K., Rix, H.-W., et al. 2003, A&A, 401, 73

Worthey, G., Faber, S. M., Gonzalez, J. J., & Burstein, D. 1994, ApJS, 94, 687

York, D. G., Adelman, J., Anderson, Jr., J. E., et al. 2000, AJ, 120, 1579

Zheng, Z., Wang, H., Ge, J., et al. 2017, MNRAS, 465, 4572

Zibetti, S., Charlot, S., & Rix, H.-W. 2009, MNRAS, 400, 1181

Appendix A: Luminosity-weighted maps
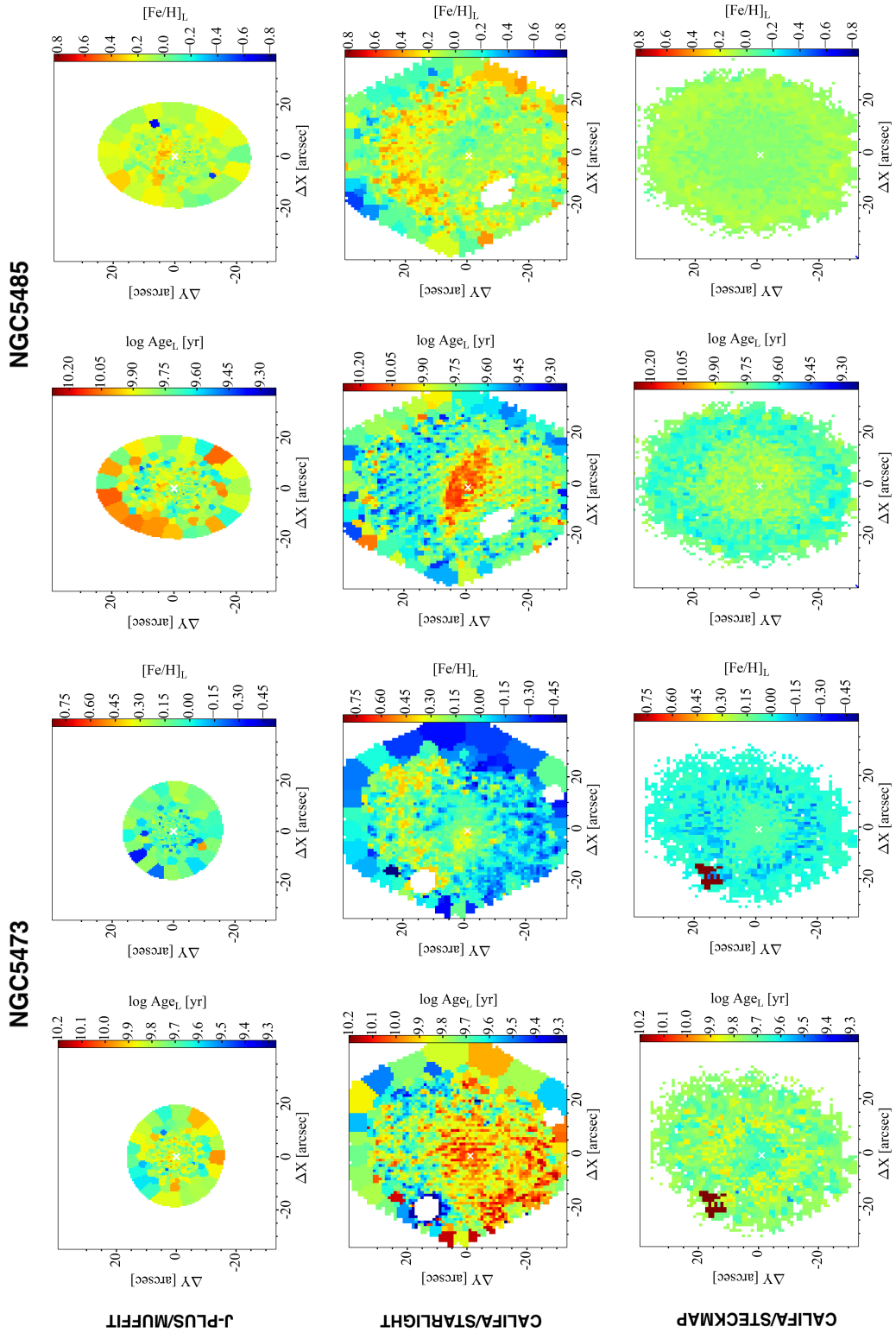
Fig. A.1. Luminosity-weighted stellar population properties maps for NGC 5473 (*first two columns*) and NGC 5485 (*last two columns*) determined by J-PLUS/MUFFIT (*first row*), CALIFA/STARLIGHT (*second row*), and CALIFA/STECKMAP (*third row*). The color range is the same for the different methods. The center of the galaxy is indicated with a white cross in each panel.